PNAS
www.pnas.org

# Supplementary Information for

## NT3-chitosan enabled de novo regeneration and functional recovery in monkeys after spinal cord injury

Jia-Sheng Rao†, Can Zhao†, Aifeng Zhang†, Hongmei Duan†, Peng Hao†, Rui-Han Wei1†, Junkui Shang†, Wen Zhao, Zuxiang Liu, Juehua Yu, Kevin S. Fan, Zhaolong Tian, Qihua He, Wei Song, Zhaoyang Yang*, Yi Eve Sun*, Xiaoguang Li*

Corresponding authors: Zhaoyang Yang*, Yi Eve Sun*, Xiaoguang Li*
Email: wack_lily@163.com (Z.Y.), yi.eve.sun@gmail.com (Y.E.S.), lxgchina@sina.com (X.L.)

**This PDF file includes:**



**Other supplementary materials for this manuscript include the following:**





www.pnas.org/cgi/doi/10.1073/pnas.1804735115

## Supplementary Information Text

## SI Materials and Methods

**NT3-chitosan tube fabrication.** Under sterile conditions, a 2% solution of poly-N-acetyl glucosamine derived from 85% deamidized chitosan (Sigma, St. Louis, USA) in 100 ml of water containing 2% acetic acid was plasticized by treatment with 1g di (hydroxyethyl) sulfoxide, which has a melting point of 112-113°C, and 1 g lithium chloride. This mixture was thoroughly stirred. A 2 mm diameter glass capillary was washed, vertically immersed in the above chitosan solution, pulled out slowly, and then dried to volatilize the solvent while keeping the tub vertical. This process was repeated until the inner and outer diameters reached 2 mm and 2-3 mm, respectively. The dried glass capillary with the chitosan tube was immersed in NaOH solution for 1h, and then in distilled water. Distilled water was changed as necessary to keep the tube from becoming alkaline. The glass capillary was then discarded, leaving a transparent chitosan tube. The tube was cut into 1 cm lengths for experimental use. The tube was sterilized by immersion in 75% ethanol overnight and the soaked with phosphate-buffered saline solution (PBS) for 10 min twice. Semifluid type I collagen was fabricated by methods previously published (1) with modifications as follows: Under sterile conditions, 25 mg of 85% deacetylated chitosan particles (Sigma, St. Louis, USA) was dissolved in 50 ml sterile deionized water at pH 7.2, allowed to swell for 6 h, and centrifuged. Then the supernatant was discarded. The swollen chitosan particles were frozen at -20°C for 24 h, and then placed at 4°C for 10 h. NT3 (Sigma, St. Louis, USA) was reconstituted to 100ug/ml in sterile cold deionized water. 100ng of NT3 were separately mixed with the above-mentioned 4°C chitosan particles solution. After stirring at 4°C for 6 h, 100 ng of NT3 loaded chitosan carriers mixture were vacuum cooled and dried. The dried chitosan particles loaded with different doses of NT3 were added to type I collagen solution at 4°C respectively stirred for 30min, centrifuged, collected and stored at 4°C for use.

**Animal models.** Thirty-eight female Rhesus Monkeys (*Macaca Mulatta*, 4-6 years old), each weighing 5±1 kg, were used in these experiments. In each experiment, numbers of animals were chosen to satisfy the statistical test requirements. Animals were divided into three groups: Uninjured, lesion control, and NT3-chitosan groups. Complete randomization was applied for group allocation and for experimental selection. One monkey with congenital spine malformation was taken out of experiments. At different time points, animals were subjected to detailed anatomical/morphological, fMRI, DTI, electrophysiological, and kinematics-based walking behavioral analyses. Other than electrophysiological studies, investigators were blinded with regard to experimental groups. All surgical and experimental procedures in monkeys were approved by and performed in accordance with the standards of the Experimental Animal Center of Capital Medical University and the Beijing Experimental Animal Association.

To perform the hemi-section lesion, monkeys were anesthetized by intramuscular injection of ketamine hydrochloric acid solution (10 mg/kg) and xylazine (5 mg/kg), and then maintained with sodium pentobarbital (20 mg/kg, i.v.gtt). After laminectomy, right thoracic spinal cord hemi-transection was performed at T8 vertebra level under an operation microscope. Right site of the spinal cord tissue (1 cm along rostral-caudal dimension and 2.35-2.75 mm along left-right direction) was excised using a scalpel. The blade was repeatedly scraped along the ventral surface

of the right side of the spinal canal, and any residual fibers at the lesion site were removed. After topical hemostatic procedures, the injured length and width of the lesion area were determined by two persons blinded to the experimental group (**Fig. S1**), and then NT3-chitosan matrix in a tubular structure matching the injury space were transplanted into the damaged site. Lesion control groups will not receive any additional intervention other than the subsequent suture of the dura, muscles and skin. Animals were placed into monkey cages individually, with environmental temperature of 23-26°C and humidity of 35-45%. Antibiotic prophylaxis continued postoperatively for 72 hours. Buprenorphine solution (50μg/100g body weight) was injected intramuscularly for 4 days after operation.

**Immunohistochemistry/Fluorescence staining.** The primary antibodies included rabbit anti-ChAT (Millipore, AB143, 1:250 dilution) labeling motor neurons, mouse anti-Neurofilament (ZSGB-BIO, ZM-0198, diluted 1:200), rabbit monoclonal anti-CD45 (Millpore, 05-1410, diluted 1:100), rabbit monoclonal anti-CD105 (Abcam, ab169545, diluted 1:50), rabbit monoclonal anti-GFAP (ZSGB-BIO, ZA-0017 diluted 1:100), are used in the study.

Monkeys from each group were sedated with ketamine (10mg/kg, i.m.) and deeply anaesthetized with pentobarbital (approximately to effect 60 mg/kg, i.v.). After transcardial perfusion with 4% paraformaldehyde in 0.1 M phosphate buffer (PB) (pH 7.4), the brain and spinal cord were carefully dissected and fixed in the same fixative at 4°C for 6-8 h, and stored in 30% sucrose in 0.1 M PBS (pH 7.4) overnight. Gross anatomical survey of the spinal cord was done under a dissecting microscope. For immunohistochemical analyses, the spinal cord tissue encompassing the lesioned area was embedded in O.C.T. (Sakura Tokyo, Japan) and longitudinally sectioned with 30-micron thickness using a leica 1850 cryostat. All sections were divided into two groups: first group for immunohistochemical staining, and second group for immunohistochemical staining-control experiments. Four monkeys were used for hematoxylin-eosin (HE) and NF staining to obtain results in **Fig. S2 and S3, Table S4**. The density of NF was analyzed quantitatively using digital images taken with an Olympus fluorescence microscope under a 10× objective. The pixel value of right half of the intact spinal cord at 2.5 mm rostral to rostral edge of the lesion covered by two objective fields was quantified and added using the "Image-Pro Plus 6.1" software as the "reference value". Within regenerated tissue, 3-4 objective fields were selected, and pixel values of each objective field were averaged. "NF fiber density index" per section was calculated by average pixel values within regenerated tissue normalized by the "reference value". We quantified 4 sections per monkey, and averaged "density indexes" were presented in **Table S4**.

Sections were washed with 0.01 M phosphate-buffered saline (PBS, pH 7.4) for three times, and incubated with the primary antibodies at 4ºC overnight. After the primary antibody incubation, the sections were incubated with appropriate secondary antibodies conjugated to various fluorescent labels, such as Texas Red dye-conjugated affinipure goat anti-mouse IgG and CyTm2-conjugated affinipure goat anti-rabbit antibodies IgG (Jackson; 1:300), at room temperature for 3h in the dark. The sections were covered with cover slips and Vectashield-mounting medium containing DAPI (Vector Laboratories), and examined under a fluorescence microscope (BX-51; Olympus, Tokyo, Japan). A normal mouse or rabbit serum was used to replace the primary antibody, serving as a control; the rest staining procedures were the same as described above.

Ten to fifteen longitudinal serial sections were selected by odd or even sequence. The numbers of cells expressing various markers were determined by counting immunopositive cells in defined areas in the lesioned/regenerated area under high magnification using a counting frame (25 μm × 25 μm) (2).

**Light and electron microscopies.** Animals were killed as described above. After transcardial perfusion with a solution of 4% paraformaldehyde and 1% glutaraldehyde, the brain and spinal

cord were carefully excised and fixed in 3% glutaraldehyde at 4°C. The rostral, middle, and caudal segments of the regenerated tissue in the tube, as well as the left uninjured cord, were immersed in 1% osmium tetroxide for 2 h, washed several times with 0.075M PBS, dehydrated in increasing concentrations of alcohol and acetone, then embedded in epoxy resin. Semith in Epon-embedded sections (1 μm) were cut horizontally, stained with 1% Toluidine blue, and observed under a light microscope equipped with a digital camera system (DP-70; Olympus, Tokyo, Japan). For transmission electron microscopy, ultrathin sections were stained with lead citrate and uranylacetate, and observed under a Philips CM 120 transmission electron microscope.

**BDA Tracing.** A frontoparietal craniotomy was performed to expose the animals' left motor cortex. BDA (10% solution in $H_2O$ (wt/vol), 10.000 molecular weight; Molecular Probes, 150 nl per site) was injected into a total of 70 points into the motor cortex of left hemispheres (3). After tracer injection, the craniotomy flap was replaced and the incision was closed. Eleven weeks after tracer injections, animals were perfused, and spinal cord encompassing the lesion site were collected for anatomic and immunohistochemical analyses.

**SEP & MEP examination.** Electrophysiological study was carried out for each group ($n = 6$ animals). Lesion control and NT3-chitosan animals were examined over 12 months after the operation. Parameters measured included somatosensory evoked potentials (SEP) and transcranial magnetic stimulation-motor evoked potentials (TMS-MEP). The S-100 Magpro Compact magnetic stimulator (Danctec Company, Denmark) was used in the experiment. It had circular stimulating coils 5 cm in diameter, with the maximal output intensity 2 Tesla. After being anaesthetized by intramuscularly injecting ketamine (50mg/kg), the limbs of experimental monkeys were abducted and fixed on a board by cloth bands. The center of the magnetic coil was placed above the motor area of cerebral cortex (We used the stereotaxic apparatus to locate the area of the cerebral motor cortex, marked the skin on the surface of the skull). The recorded contraction of the target muscle was taken as the stimulation intensity, that is, 40-70% of the maximum output intensity. Normally 60% of the maximum stimulation input was used for TMS-MEP analyses. The recording electrode was placed on the muscle belly surface of tibialis anterior muscle of the bilateral hindlimbs, the reference electrode at the distal end of 2 cm, and the ground electrode was place on the belly. The signals were amplified and recorded by a Keypoint-II bichannel evoked potential/electromyography with filter pass band of 2 Hz-10 kHz and amplifier sensibility of 0.1mV/D. At room temperature of 24-26°C, the experiment was carried out repeatedly. The onset latency and the amplitude from Negative to Positive (from N to P) were measured, and the latencies of the motor responses were normalized to the height of the subject (4).

Before the TMS-MEP test for the experimental animals, we determined the motor threshold. To determine the threshold, the stimulus intensity was decreased to the level of no response, and the intensity of the stimulus was increased to the next highest level by increments of 10%, until a response was obtained (5, 6). Each trial was replicated. TMS-MEP with amplitude of ≥ 15uV was considered as suprathreshold (5, 6).

We also examined the somatosensory evoked potential of the above-mentioned monkeys. SEP was measured by a Keypoint bichannel evoked potential/electromyography. The stimulating electrodes included positive and negative ones. A positive electrode was inserted into the muscle belly of tibialis anterior muscle of the bilateral hindlimbs to a depth of 3-5 mm, with the negative electrode located at the distal end, 2 cm away. Successive stimulation was given at tibialis anterior muscle of the bilateral hindlimbs, at the stimulating intensity of 20 mA (that is to make the toes of the hindlimbs slight move, duration time of 0.2 ms, amplifier sensitivity of 10 uV/D, filter pass band of 20Hz-3kHz, with sweep length set to 80-100 ms, for 200 times on average. SEPs were recorded on the skull surface above the sensory area of the cerebral cortex (We used the stereotaxic apparatus to locate the area of the cerebral somatosensory cortex, marked the skin

on the surface of the skull), and the latency (P1) and amplitude (P1-N1) were measured, while keeping the distance between stimulating electrodes and recording electrodes constant.

After the SEP and MEP examinations, randomly selected 5 monkeys from NT3-chitosan group were anaesthetized with ketamine. Dura mater was opened and the T8-10 spinal cord was exposed. For 2 monkeys, the 1 cm-long healthy spinal cord contralateral to the tube was cut and removed. The surgical blade was repeatedly scraped along the ventral surface of the spinal canal, and any residual fibers at the lesion site were removed by aspiration. Then a cotton ball that had been immersed in liquid paraffin was inserted. For the other 3 monkeys, the regenerated spinal cord tissue in the tube was cut and removed. The surgical blade was repeatedly scraped along the ventral surface of the spinal canal. Then a cotton ball that had been immersed in liquid paraffin was inserted. MEP and SEP were recorded on both sides of the above monkeys three months after resection, using the same parameters as mentioned above.

**Anesthesia for MRI examinations.** Animals of each group ($n$ = 3-5 animals) were anesthetized for MRI scanning. Each rhesus monkey was given ketamine hydrochloric acid solution (10 mg/kg, i.m.) and atropine sulfate injections (0.05 mg/kg, i.m.) before MRI scanning to induce anesthesia and to decrease bronchial and salivary secretions. Anesthesia was maintained during the scan by continuous administration of propofol (0.25 mg/kg/min, i.v.gtt) and additional 5 mg ketamine every 30 min. During fMRI, the level of anesthesia was monitored periodically for following reactions as the standard: i.e., no somatic movement when toes were pinched; corneal reflex disappeared while the heart rate was kept higher than 70 times/min; and respiration rate was higher than 20 times/min (7, 8). During DTI, animals were anesthetized by Xylazine hydrochloride solution (0.1 mg/kg, i.m.).

**fMRI Stimulation.** Innocuous heat stimulation was used for fMRI somatosensory test. For somatosensory test, a laser stimulator was used for innocuous thermal stimulation (42°C). The medial cutaneous surface of the glabrous foot in bilateral hindlimbs was stimulated. The block design was adopted with a 20 s stimulation period, followed by a 20 s rest period. The stimulation blocks and the rest blocks alternated and repeated 4 times. Before the first stimulation period, an extra 20 s was added to obtain the baseline hemodynamic response (9). The stimulated regions were arranged in a pseudo-randomized order. Between different stimulation regions, a 5 min rest interval was applied to allow the hemodynamic response to return to the baseline.

**MRI data acquisition.** All MRI research was accomplished with the Siemens 3T MR (Siemens, Erlangen, Germany). Structural and functional images of brain were acquired with a custom-made primate four-channel transmitter and receiver coil. The spine coil received MRI and DTI signals from the spinal cord. The BOLD signals were obtained with the gradient echo–echo planar imaging sequence (GE-EPI), and set as follows: TR = 2000 ms, TE = 30 ms, matrix = 64 × 64, field of view (FOV) = 128 × 128 $mm^2$, flip angle = 90°, 25 consecutive slices of the axial image covered the entire brain, and voxel spatial resolution was 2 × 2 × 2 $mm^3$. Before each functional imaging scan, 4 s of empty scanning was adopted to avoid the magnetic field heterogeneity at the beginning of the scanning. Each scanning period lasted 3 min 4 s, and 90 volumes of EPI data were acquired.

The 3D magnetization prepared rapid acquisition gradient echo sequence (MPRAGE) was used to obtain high-resolution anatomical structure images, with the following parameters: TR = 1520 ms, TE = 4.42 ms, flip angle = 15°, and TI = 520 ms, same centering to functional data, and 180 contiguous slices covering the entire brain; the voxel spatial resolution was 1.0 × 0.5 × 0.5 $mm^3$.

The single-shot spin-echo echo planar imaging (SE-EPI) was used for the spinal DTI sequence with two b values (b = 0 and 1000s/$mm^2$). A twice-refocusing pulse sequence was used to minimize eddy current effects (10). Axial-orientation diffusion-weighted (DW) images were acquired using the following parameters: TR = 4500 ms, TE = 104 ms, matrix = 128 × 128, FOV

= 196× 196 $mm^2$, 25 contiguous slices covering the lesion area. Nominal voxel size is 1.5 × 1.5 × 2 $mm^3$. Data were acquired six times in 13 gradient directions to enhance the signal-to-noise ratio. Saturation bands were set on monkey's chest and abdomen to reduce movement artifacts. The Siemens generalized autocalibrating partially parallel acquisitions (GRAPPA) imaging system was used with acceleration factor of 2 to shorten the echo train length. In this method, geometric distortions induced by susceptibility artifacts can be greatly reduced while keeping the SNR virtually the same (11). To limit the extent of susceptibility artifacts, the readout bandwidth was adjusted to produce the minimum possible echo spacing (12), with the bandwidth set to 1396 Hz and the echo train spacing to 0.82ms.

Structural images were obtained with proton density (PD) sequence in the same orientations with DTI. The imaging parameters were as follows: TR = 3050 ms, TE = 11 ms, flip angle = 149°, matrix = 320 × 320, and 27 consecutive slices of axial images covering the SCI region. The voxel spatial resolution was 0.6 × 0.6 × 2 $mm^3$. The saturated band was set in the chest and abdominal cavity to reduce physiologic motion artifacts.

**fMRI data processing.** All fMRI data were processed with Statistical Parametric Mapping (SPM) version 8 (http://www.fil.ion.ucl.ac.uk/spm/). The first three volumes of every scan were excluded to avoid possible instabilities of the initial MRI signal. For the remaining images, the middle slice of each volume was used as the reference for rearrangement to fix the acquisition time delay. Rigid transformation of six parameters registered all data on the first image to fix motion artifacts (13). After motion correction, data were registered in accordance with anatomical structural images of each monkey and then standardized using published monkey MRI brain atlas (14, 15). Finally, a 3 mm isotropic Gaussian filter was used for image smoothing. We built up the activated regression analysis through the convolution block design paradigm with canonical hemodynamic response function. The activation map was generated using the SPM general linear model. The low-frequency signal drift was removed with a high-pass filter at 1/100Hz (16). The spherical ROI with 4 mm radius were positioned on bilateral medial primary somatosensory cortical regions (S1) based on hindlimb sensory representation using monkey MRI brain atlas (15, 17) and confirmed by actual experiment using uninjured monkeys (**Fig. 5**). The central coordinates of the sphere were 7,6,38 (right side) and -7,6,38 (left side) in the MNI space (**Fig. S7**).

**DTI data processing.** DTI scans were processed and analyzed by means of dedicated MedINRIA software (http://www-sop.inria.fr/asclepios/software/MedINRIA). Eddy current distortions were corrected using 12-mode linear affine intrasubject registration of all DW scans, with an average of six b0 images as reference. The non-rigid deformation field was estimated to register the EPI on the structural volume. For each direction in all DW scans, a deformation field was calculated in the same way and applied accordingly. After processing, eigenvalues in three perpendicular directions were derived from every pixel to calculate the FA (18). The directions of eigenvector related to the largest eigenvalues were set to the main direction of local neural fibers (19). A background removal threshold of 0.10 was set to exclude non-positive voxels and any significant noise; smoothing of the interpolated fiber was set to 20% and the minimum fiber length was set to 1 cm for continuous fiber reconstruction. FA values in the ROIs, which were located at the surgical area, rostral, and caudal sites were extracted (**Fig. S10 and Fig. 7*E***) and were used for statistical comparisons.

**Kinematics analyses of bipedal locomotion.** The bipedal locomotion of animals was characterized by gait test. The study methods have been published previously (20, 21). In brief, monkeys in each group ($n$ = 3-5 animals) performed bipedal locomotion on a treadmill under restrained condition by a customized device (**Fig. S8*B***). The animals wore customized stretchy pants to avoid irritation and volunteering removal of the reflective markers. All behaviorally-

tested animals were trained 3 times at healthy stage to adapt the treadmill walking/stepping. Both lesion control and NT3-chitosan groups did not undergo any training after operations. 16-point reflective markers were fixed on the anterior superior iliac spines, posterior superior iliac spines, the 2/3 of femur, knees joints, tibia midpoint, ankle joints, heels, and the second metatarsophalangeal joint (MTP joint) in the bilateral hindlimbs; relative displacement was assured not to occur. The Vicon system (Vicon 8, Oxford Metrics Limited, UK) was used for gait data acquisition of the hindlimbs, with a sampling frequency of 100 Hz. In the test, animals walked on a treadmill at a speed of 0.22 m/s. The data for continuous steps were obtained for subsequent processing and analysis.

The kinematics analyses were performed as follows: (i) the real-time 3D coordinate data of each reflective marker was acquired through the Vicon system when the animal was stepping; (ii) gait datasets were calculated using Matlab (MathWorks, Natick, MA, USA) to extract 127 gait parameters (including characteristic parameters and correlation coefficient) of each gait cycle (**Table S5**) and normalized (22); (iii) The gait parameters in three animal groups "Uninjured", "Lesion control" and "NT3-chitosan" were clustered using R package "hclust" with the method of "average". The normalized parameter values were first averaged for each group and the heatmap and clustering were prepared with "heatmap.2" (23-25); (iv) 12 clinically relevant parameters was selected based on the following criterion: these parameters shall directly reflect the degree of functional recovery of paralyzed hindlimb with reproducible spatiotemporal measures. All data of these parameters in three groups were analyzed and displayed.

**Statistical analyses.** For lesion size analysis, a two-tailed independent sample t-test was used to compare lesion areas between lesion control and NT3-chitosan groups. The one-sample Kolmogorov-Smirnov tests showed that data did not depart significantly from normality. $P < 0.05$ was considered statistically significant. All values are presented as mean ± SEM.

For electrophysiology analyses, one-way analysis of variance (ANOVA) using the Bonferroni test (multiple comparison for three groups), or two-tailed independent sample t-tests, were used to determine statistical differences between groups. The Shapiro-Wilk test was used for data normality analysis, and the Levene's test was used to test for homogeneity of variance. $P < 0.05$ was taken to indicate statistically significant differences. All values are presented as mean ± SEM.

For fMRI analyses, group analyses were performed by using statistical functions, which were integrated in SPM8. $P < 0.05$ with Gaussian Random Field Theory (GRF) multiple comparisons correction was considered to be statistically significant. To compare the BOLD signal change values among three groups (uninjured, lesion control, and NT3-chitosan), one-way ANOVA using the Bonferroni test (Homogeneity of variance) or Dunnett's T3 test (Inhomogeneity of variance) were used. The one-sample Kolmogorov-Smirnov tests showed that data did not depart significantly from normality. The Levene's test was used to test for homogeneity of variance. $P < 0.05$ was considered statistically significant. All values are presented as mean ± SEM.

For DTI analyses among three groups (uninjured, lesion control, and NT3-chitosan), one-way ANOVA using the Bonferroni test (Homogeneity of variance) or Dunnett's T3 test (Inhomogeneity of variance) were used to compare FA values. The one-sample Kolmogorov-Smirnov test was used for FA normality analysis, and the Levene's test was used to test for homogeneity of variance. A nonparametric Kruskal-Wallis ANOVA was used to calculate percentage of rostral-caudal voxels. To compare data between lesion control and NT3-chitosan groups at different time points, two-tailed independent sample t-tests or two-tailed Mann-Whitney U-test were used. The one-sample Kolmogorov-Smirnov test was used for data normality analysis. Additional two-way ANOVAs were also performed to compare data between lesion control and NT3-chitosan groups at different time points. FA values / percentage of rostral-caudal voxels were set as dependent variables; groups and time points were fixed variables. $P < 0.05$ was considered statistically significant. All values are presented as mean ± SEM.

For gait analyses, two-tailed Mann-Whitney U-test was used for comparisons between two groups. One-way ANOVA using the Bonferroni test (Homogeneity of variance) or Dunnett's T3 test (Inhomogeneity of variance), or nonparametric Kruskal-Wallis test, were used for comparison between multiple groups. The one-sample Kolmogorov-Smirnov test was used for data normality analysis, and the Levene's test was used to test for homogeneity of variance. $P < 0.05$ was considered statistically significant. All values are presented as mean ± SEM.

A

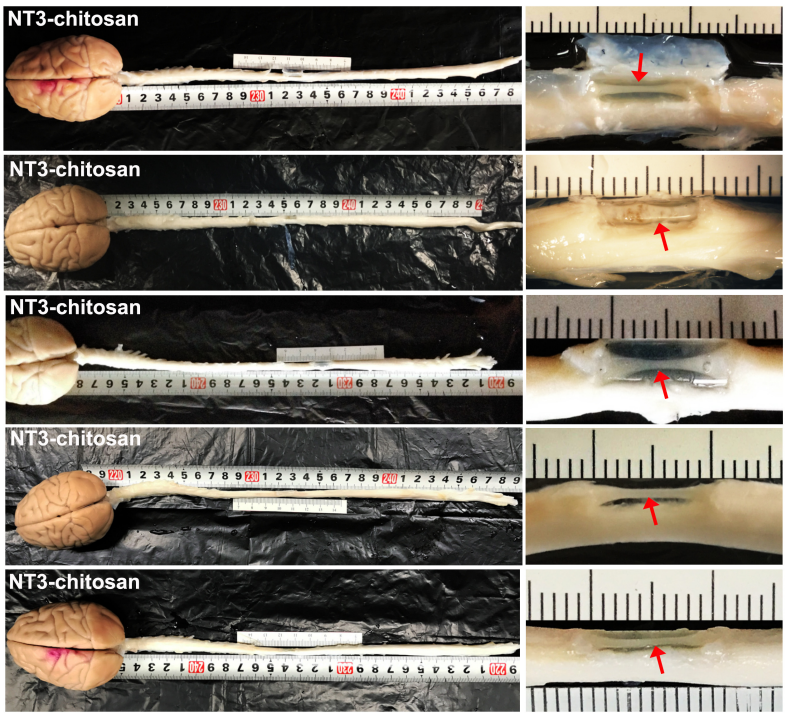


B

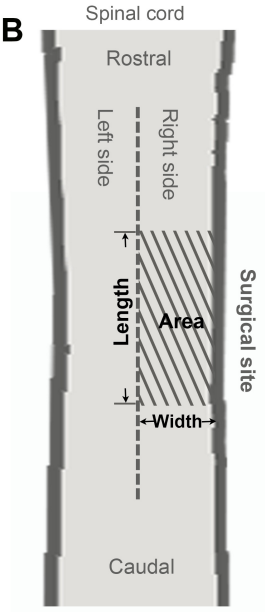


C

Detailed lesion size

| Monkey No. | Group | Length(mm) | Width(mm) | Area(mm²) |
|---|---|---|---|---|
| #1 | LC (n = 12) | 10.00 | 2.43 | 24.30 |
| #2 | | 10.00 | 2.66 | 26.60 |
| #3 | | 10.00 | 2.75 | 27.50 |
| #4 | | 10.00 | 2.47 | 24.70 |
| #5 | | 10.00 | 2.46 | 24.60 |
| #6 | | 10.00 | 2.66 | 26.60 |
| #7 | | 10.00 | 2.55 | 25.50 |
| #8 | | 10.00 | 2.70 | 27.00 |
| #9 | | 10.00 | 2.35 | 23.50 |
| #10 | | 10.00 | 2.58 | 25.80 |
| #11 | | 10.00 | 2.49 | 24.90 |
| #12 | | 10.00 | 2.46 | 24.60 |
| #13 | NT3 (n = 20) | 10.00 | 2.35 | 23.50 |
| #14 | | 10.00 | 2.70 | 27.00 |
| #15 | | 10.00 | 2.35 | 23.50 |
| #16 | | 10.00 | 2.68 | 26.80 |
| #17 | | 10.00 | 2.51 | 25.10 |
| #18 | | 10.00 | 2.38 | 23.80 |
| #19 | | 10.00 | 2.47 | 24.70 |
| #20 | | 10.00 | 2.53 | 25.30 |
| #21 | | 10.00 | 2.34 | 23.40 |
| #22 | | 10.00 | 2.45 | 24.50 |
| #23 | | 10.00 | 2.70 | 27.00 |
| #24 | | 10.00 | 2.55 | 25.50 |
| #25 | | 10.00 | 2.75 | 27.50 |
| #26 | | 10.00 | 2.38 | 23.80 |
| #27 | | 10.00 | 2.66 | 26.60 |
| #28 | | 10.00 | 2.49 | 24.90 |
| #35 | | 10.00 | 2.60 | 26.00 |
| #36 | | 10.00 | 2.38 | 23.80 |
| #37 | | 10.00 | 2.54 | 25.40 |
| #38 | | 10.00 | 2.49 | 24.90 |

D

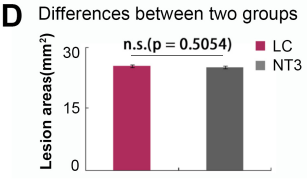

**Fig. S1.** Gross anatomy of regenerated neural tissue from 5 monkeys with NT3-chitosan treatment and detailed information of the lesion size for all animals. (*A*) Red arrows point at regenerated neural tissues. (*B*) The schematic diagram illustrates how lesion size is measured. Animal numbers and corresponding lesion size (length, width, and areas) were shown for 12 lesion control (LC) and 20 NT3-chitosan (NT3) animals. Lesion areas between LC and NT3 groups were compared by using a two-tailed independent sample t-test, and no significant difference were found. Error bars represent the mean ± SEM.

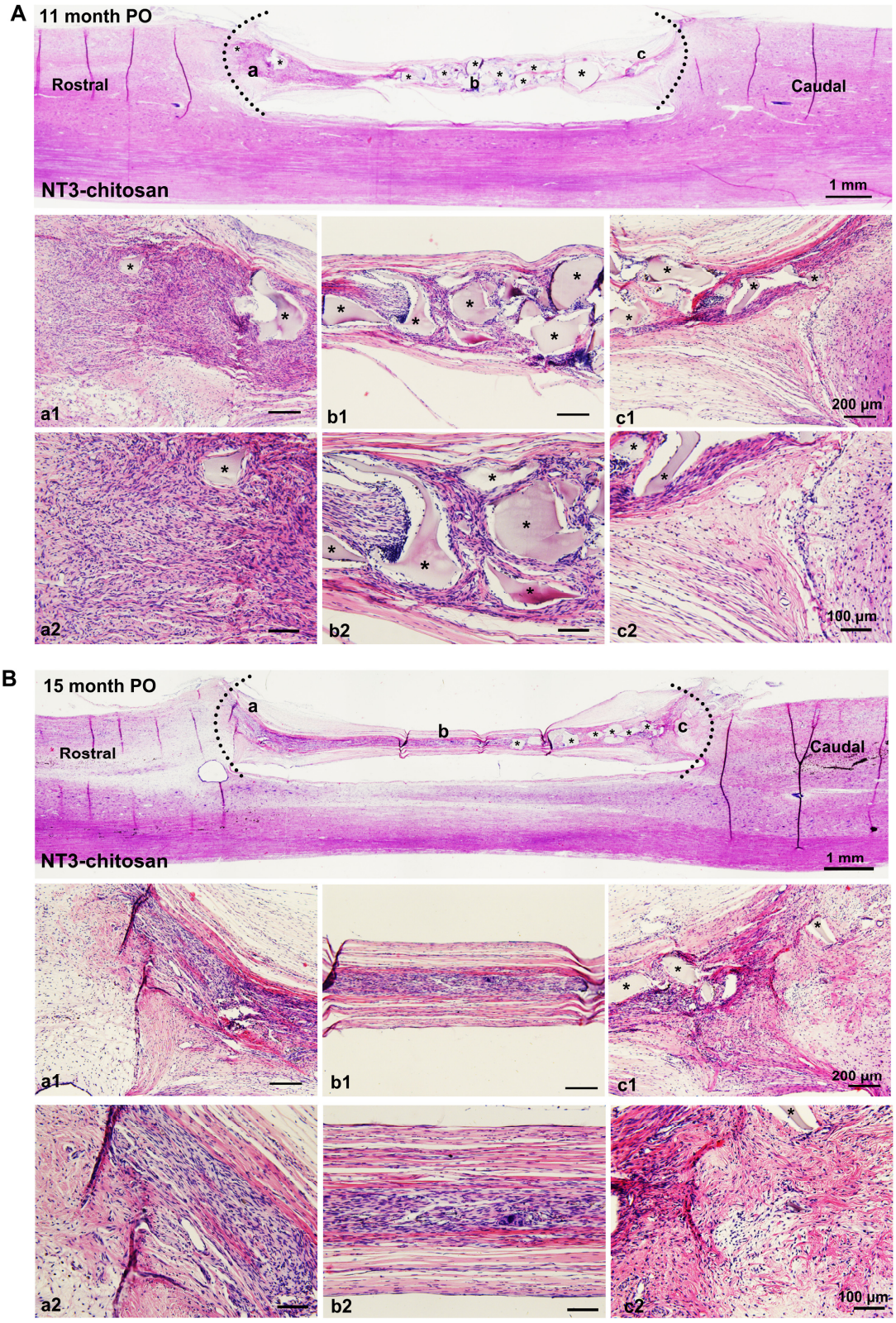
A
11 month PO
Rostral
a
b
c
Caudal
NT3-chitosan
1 mm
a1
b1
c1
200 μm
a2
b2
c2
100 μm
B
15 month PO
Rostral
a
b
c
Caudal
NT3-chitosan
1 mm
a1
b1
c1
200 μm
a2
b2
c2
100 μm

**Fig. S2.** HE staining of regenerated monkey spinal cord bridging neural tissues with treatment of NT3-chitosan at 11month (*A*) and 15month (*B*) post operation (PO). (*a'*, *a'1*, *a'2*) represent a serial magnification of the entry area: (*b'*, *b'1*, *b'2*), middle area, and (*c'*, *c'1*, *c'2*), exit area. (*) represent not-yet-degraded NT3-chitosan material. It is obvious that when there are still quite some non-degraded materials, axons and cells have to detour around the particles (*A*), and after degradation of the material, longitudinally ordered fibers and cell tracks can be seen (*B*). In addition, the final remodeled neural tissue display a two-end funnel like shape.

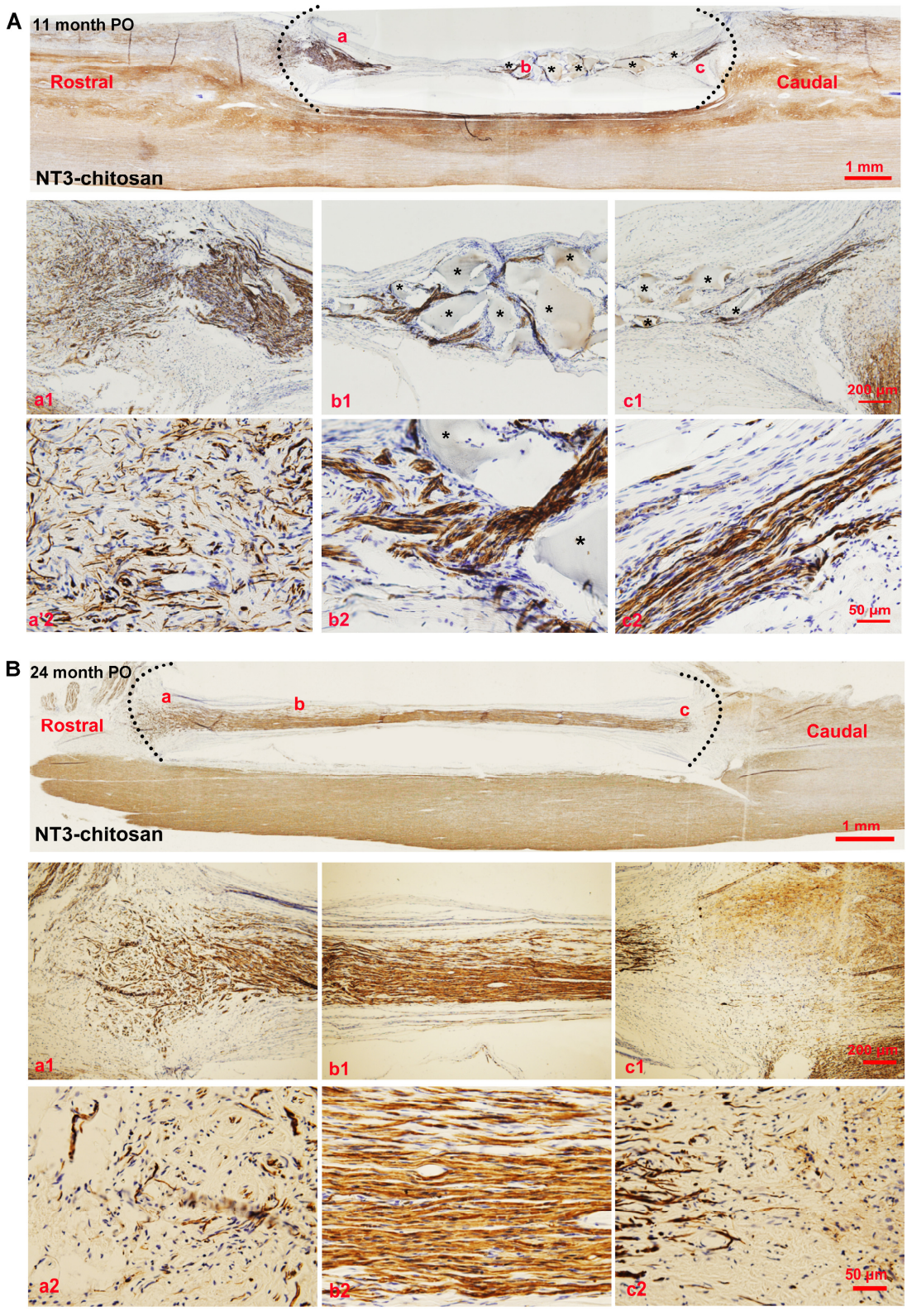
A
11 month PO
Rostral
Caudal
a
b
c
NT3-chitosan
1 mm
a1
b1
c1
200 μm
a2
b2
c2
50 μm
B
24 month PO
Rostral
Caudal
a
b
c
NT3-chitosan
1 mm
a1
b1
c1
200 μm
a2
b2
c2
50 μm

**Fig. S3.** NF and DAPI (blue) staining of regenerated monkey spinal cord bridging neural tissue after NT3-chitosan treatment at 11month (*A*) and 24month (*B*) post operation (PO). (*a'*, *a'1*, *a'2*, *a'3*) represent a serial magnification of the entry area: (*b'*, *b'1*, *b'2*, *b'3*), middle area, and (*c'*, *c'1*, *c'2*, *c'3*), exit area. (*) represent not-yet-degraded NT3-chitosan material. It is obvious that when there are still quite some non-degraded materials, axons have to detour around the particles (*A*), and after degradation of the material, longitudinally ordered fibers can be seen (*B*). In addition, the final remodeled neural tissue display a two-end funnel like shape.

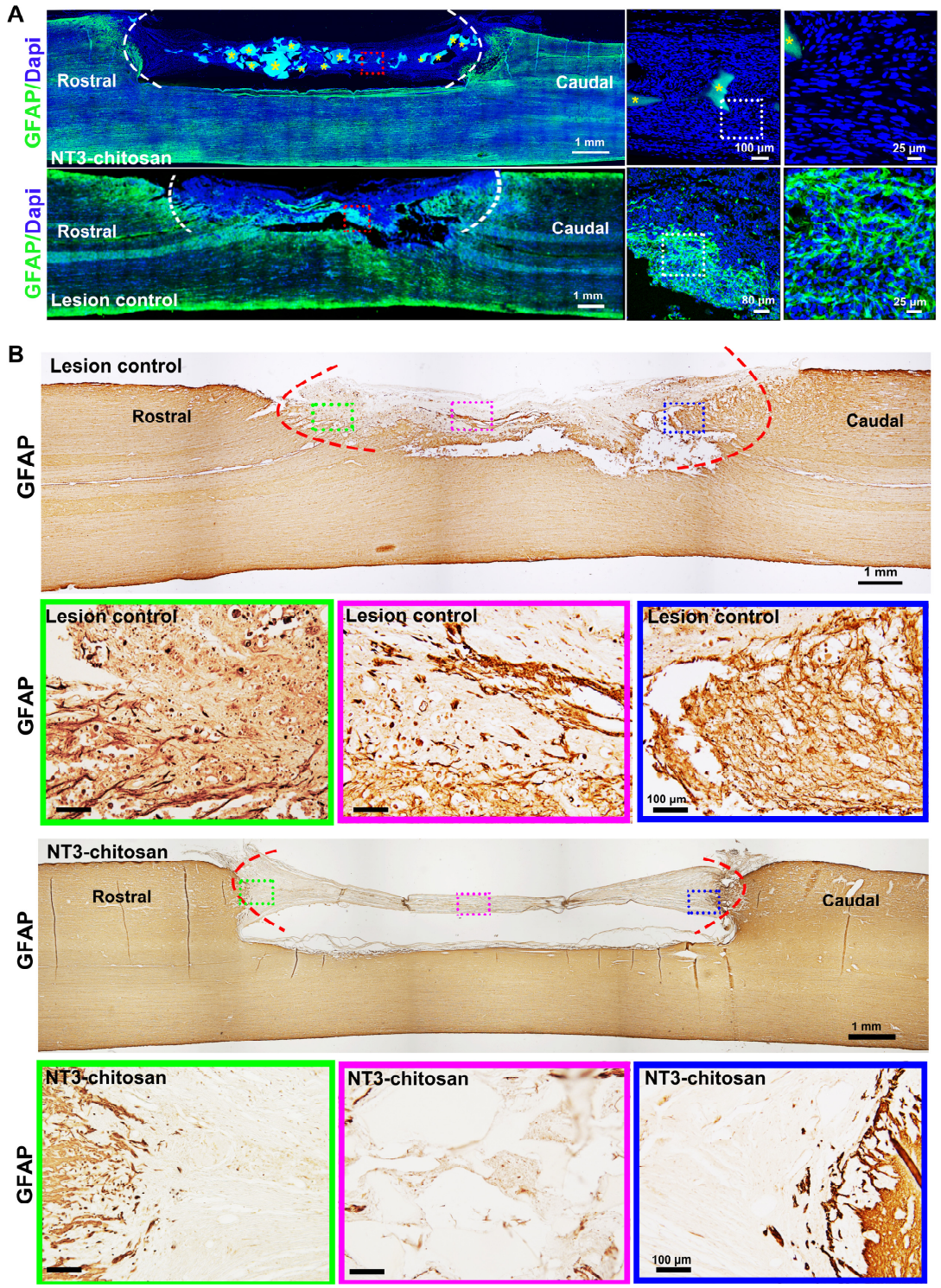


**Fig. S4.** NT3-chitosan treatment reduced GFAP immunoreactivities. (*A*) GFAP immunofluorescent immunostaining results of NT3-chitosan treated monkey and lesion control monkey spinal cord over one year after the initial operation. (*B*) GFAP immunostaining results of

NT3-chitosan treated monkey and lesion control monkey spinal cord. Three ROI (green, pink, and blue boxes) were demonstrated with higher magnifications. Clearly NT3-chitosan substantially reduced GFAP immunoreactivities in lesion area, indicative of reduced glial scaring. (*) represent not-yet-degraded NT3-chitosan material.

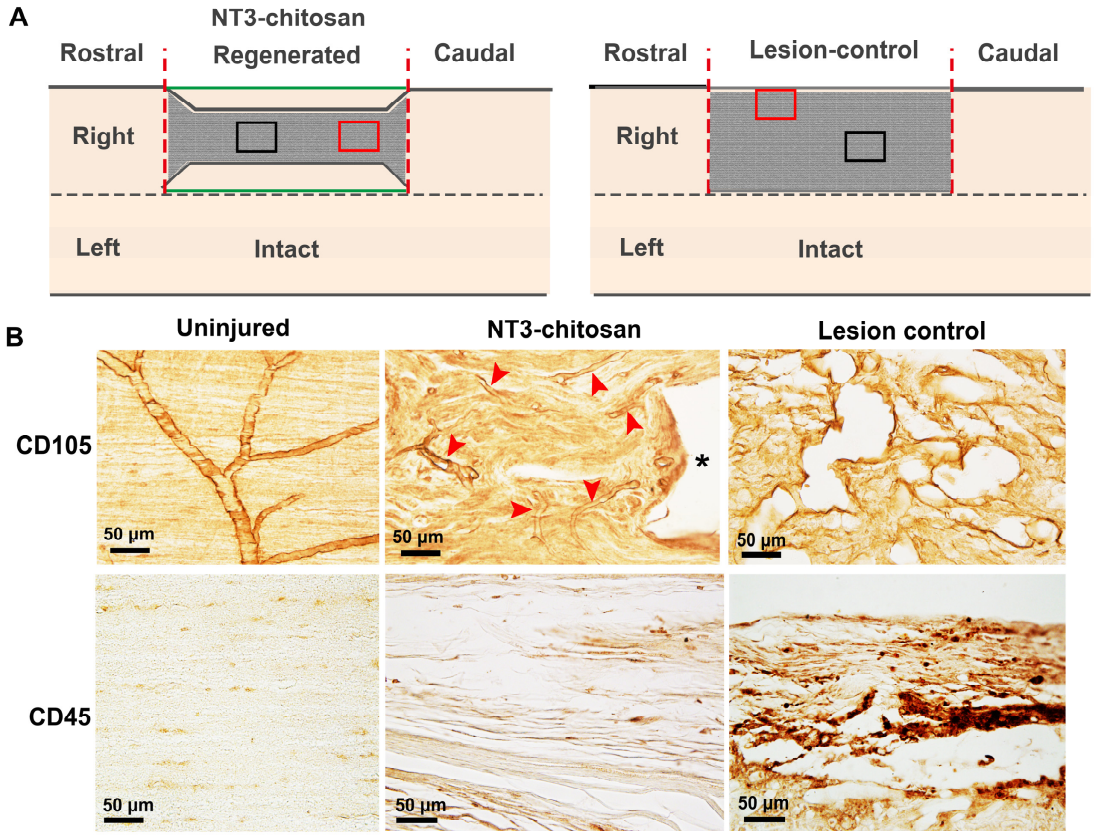


**Fig. S5.** NT3-chitosan treatment reduced inflammation (CD45 labeling), and enhanced vascularization (CD105 labeling). (*A*) Schema showing the positions of ROIs in (*B*) Black ROI represents image areas for CD105 staining in (*B*), and red ROI for CD45 staining. CD45 is a marker for leukocytes, and CD105 could label blood vessels. (*B*) Clearly demonstrating NT3-chitosan is anti-inflammatory (reduced CD45 signals) and provascularization (appearance of CD105 blood vessel like structures, shown by red arrowheads).

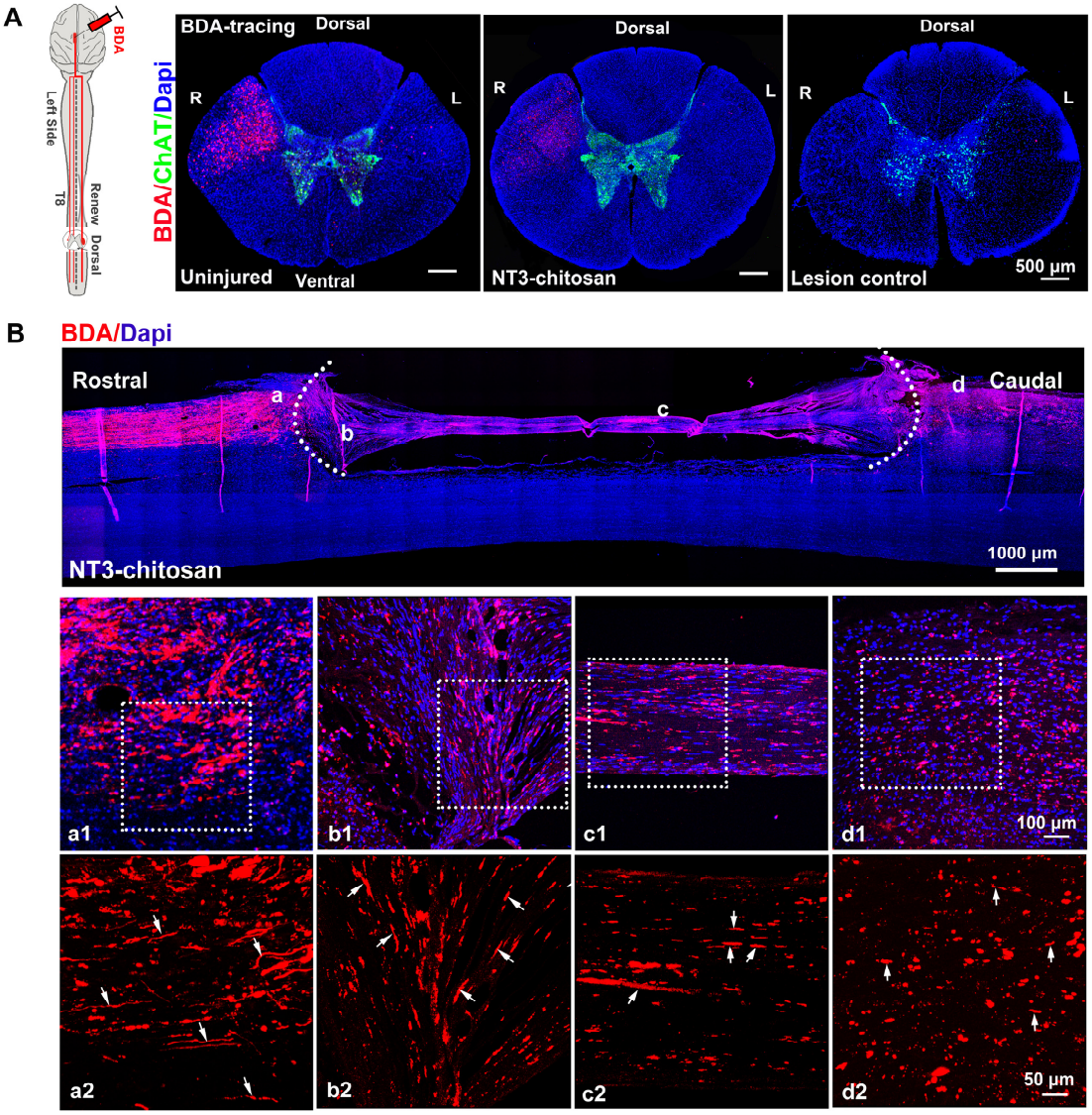


**Fig. S6.** The BDA tracing demonstrating robust axonal regeneration elicited by NT3-chitosan. (*A*) A schema demonstrating BDA tracing experiment. BDA tracing demonstrated CST regenerations with NT3-chitosan treatment over two years post operation. Right panels, spinal cord trans-sections about 15 mm caudal to the distal lesion edge were analyzed for BDA signals and motor neuronal marker ChAT. (*B*) Longitudinal section of BDA labeling.

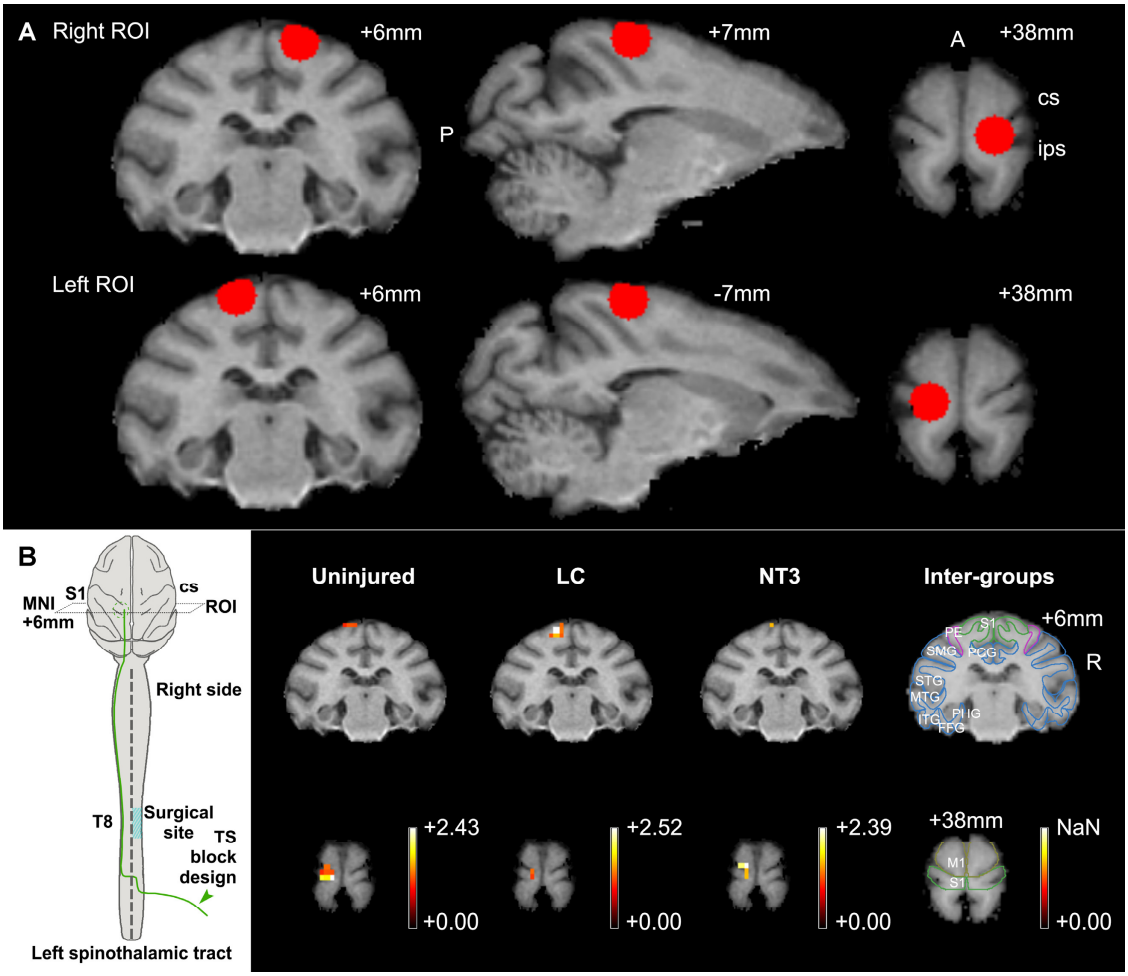


**Fig. S7.** The regions of interests (ROIs) were defined and no significant changes were observed in the unaffected left side of primary somatosensory cortex after stimulations of right hindlimbs. (*A*) The regions of interests (ROIs) were defined in the bilateral primary somatosensory cortex. Based on the Rhesus Macaque atlas (15, 17), two spherical ROIs with 4 mm radius were constructed to represent left and right hindlimb receptive fields. The center coordinates of ROIs were 7,6,38 (right side) and -7,6,38 (left side) in the Montreal Neurological Coordinates space. (*B*) Diagram illustrating fMRI experiments. Averaged fMRI signals were superimposed onto coronal and axial structural images within uninjured, lesion control (LC), and NT3-chitosan (NT3) groups, respectively. Each group displayed significant activation in the left S1 area representing the right hindlimb receptor field upon cold stimulation ($P < 0.05$, GRF multiple corrected). The schematic diagram of brain structures was overlapped on the coronal and axial images. Each gray matter site was indicated. Results showed no obvious changes among three groups ($P < 0.05$, GRF multiple corrected). Color scales indicate t values. MNI coordinates were given in the figure. (abbreviations: P, posterior; A, anterior; cs, central sulcus; ips, intraparietal sulcus) R, right; PE, sensory association cortex; PCG, posterior cingulate cortex; SMG, supramarginal gyrus; STG, superior temporal gyrus; MTG, middle temporal gyrus; ITG, inferior temporal gyrus; FFG, fusiform gyrus; PHG, parahippocampal gyrus; S1, primary somatosensory cortex; MNI, Montreal Neurological Coordinates; T, thoracic vertebra; TS, temperature stimulation).

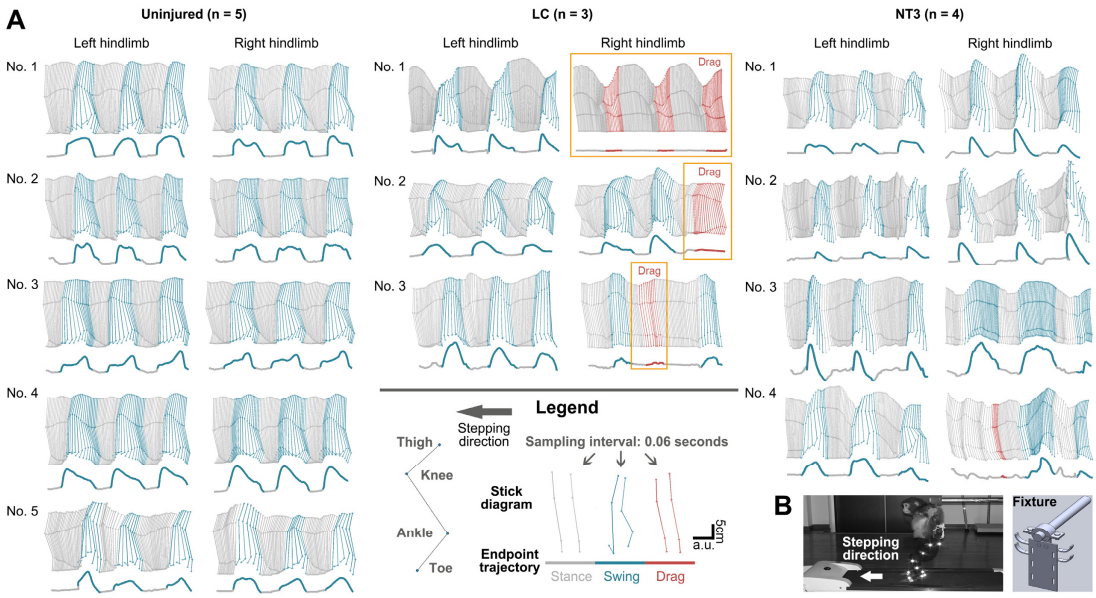


**Fig. S8.** NT3-chitosan transplantation improved locomotion in NT3-chitosan group. (*A*) Representative stick diagram decompositions (60 ms between sticks) were shown for five uninjured, three lesion control (LC) and four NT3-chitosan (NT3) treated monkeys. For each panel stick plots of hindlimb motion were shown together with color-coded trajectories of the hindlimb endpoint (below the stick-plots). Dragging was indicated by orange boxes. Continuous stepping occurred in the same space system because animals were placed on the treadmill. The distance between each step is arbitrarily assigned. (*B*) Monkeys were fixed on a treadmill, and the spatial locations of the fluorescent markers were recorded when stepping. The fixture was shown at the right bottom.

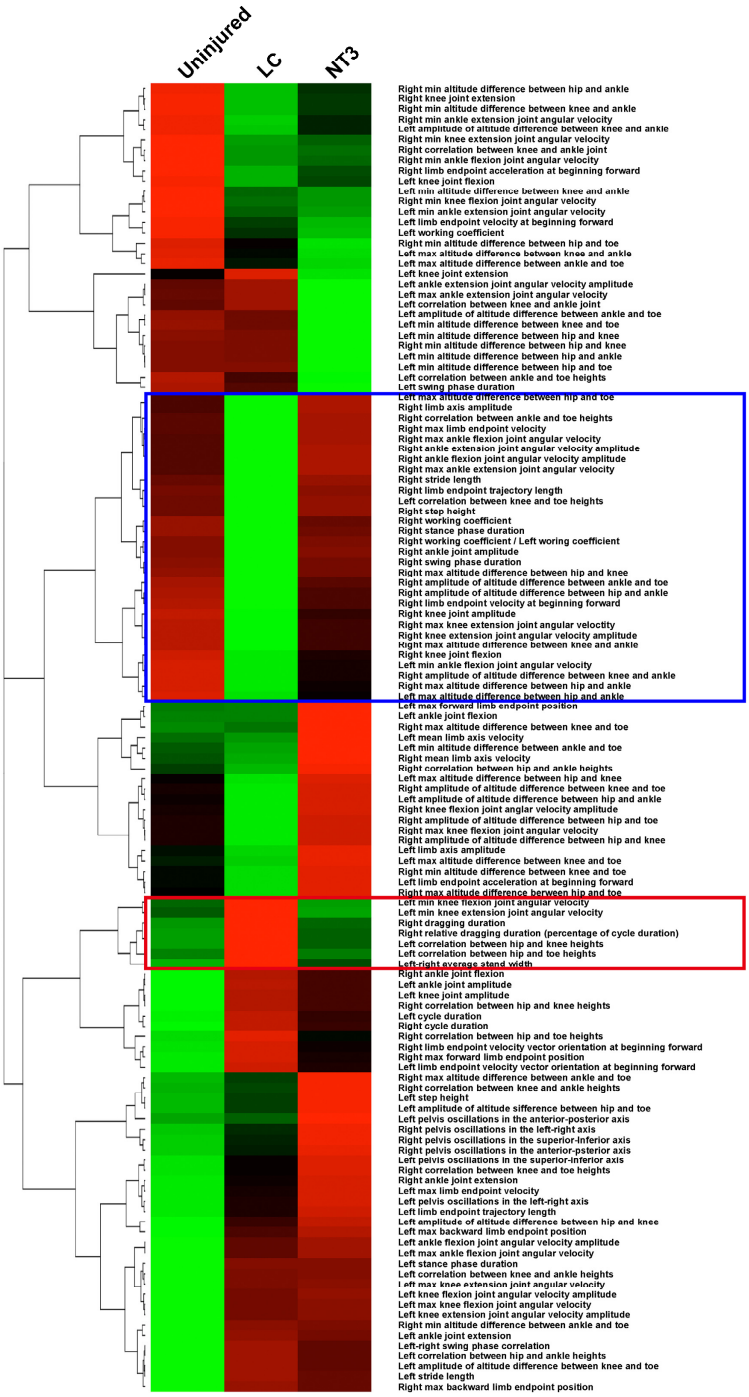


**Fig. S9.** Non-supervised and unbiased hierarchical clustering of 127 kinematics walking parameters, representing all gait cycles. A heatmap coupled with clustering analysis for 127 walking behavioral parameters for three animal groups “Uninjured”, “Lesion control” (LC), and “NT3-chitosan” (NT3). Blue and Red boxes represent parameters that are most clinically relevant.

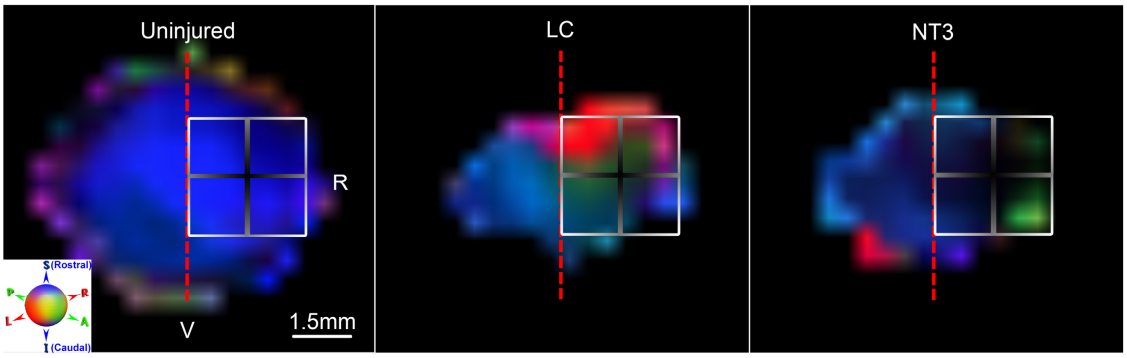


**Fig. S10.** The schematic diagram of the locations of voxels acquired within spinal cord for DTI analyses. In uninjured, lesion control (LC), and NT3-chitosan (NT3) animals, the diffusion information was extracted in 4 voxels in the right side of the spinal cord at each level analyzed along the rostral-caudal axis. Color in the processed images represented the main diffusion direction. White panes indicate the used voxels. V, ventral; R, right.

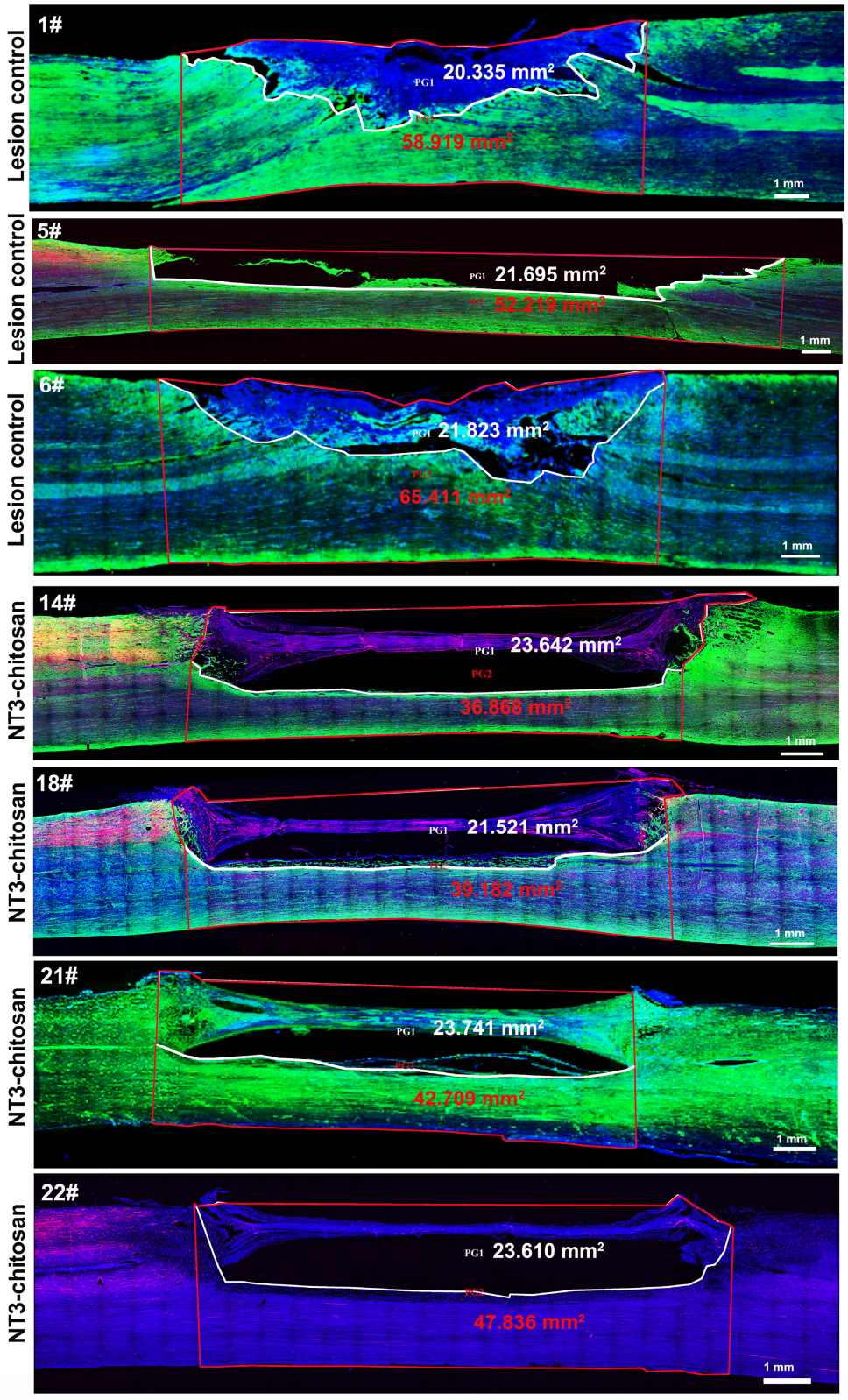
Lesion control
1#
PG1 20.335 mm²
PG2 58.919 mm²
1 mm
Lesion control
5#
PG1 21.695 mm²
PG2 52.219 mm²
1 mm
Lesion control
6#
PG1 21.823 mm²
PG2 65.411 mm²
1 mm
NT3-chitosan
14#
PG1 23.642 mm²
PG2 36.868 mm²
1 mm
NT3-chitosan
18#
PG1 21.521 mm²
PG2 39.182 mm²
1 mm
NT3-chitosan
21#
PG1 23.741 mm²
PG2 42.709 mm²
1 mm
NT3-chitosan
22#
PG1 23.610 mm²
PG2 47.836 mm²
1 mm

**Fig. S11.** Demarcation of lesion areas and corresponding total areas (lesion plus speared areas) more than one-year post operation, for correlation analyses with animal walking behavior.

**Table S1. Lesion control monkeys' detailed information (bedsore rate: 58.33%).**

| Monkey | Type | Bed-sore | Dead time post-surgery | Cause of death | Electro-physiology | MRI | Behavioral analysis | Histology | Regenerated (Histology/MRI/ Behavior) |
|---|---|---|---|---|---|---|---|---|---|
| #1▲★ | Lesion control | No | 2 years and 1 month | Perfusion | No | Yes | Yes | Yes | No |
| #2 ★ | Lesion control | Yes | 1.5 months | Unknown | No | Yes | No | No | No |
| #3 | Lesion control | Yes | 1.3 months | Unknown | No | Yes | No | No | No |
| #4 ★ | Lesion control | No | 1 month | Perfusion | No | Yes | No | Yes | No |
| #5 ★ | Lesion control | No | 3 years | Perfusion | No | Yes | Yes | Yes | No |
| #6▲★ | Lesion control | No | 2 years and 2 months | Perfusion | No | Yes | Yes | Yes | No |
| #7 | Lesion control | Yes | 1 year and 3 months | Perfusion | Yes | No | No | Yes | No |
| #8 | Lesion control | No | 2 years and 1 month | Perfusion | Yes | No | No | Yes | No |
| #9 | Lesion control | Yes | 1 year and 1 month | Perfusion | Yes | No | No | Yes | No |
| #10 | Lesion control | Yes | 1 year and 9 months | Perfusion | Yes | No | No | Yes | No |
| #11 | Lesion control | Yes | 1 year and 8 months | Perfusion | Yes | No | No | Yes | No |
| #12 | Lesion control | Yes | 1 year | Perfusion | Yes | No | No | Yes | No |

★, additional Behavioral analysis was performed before surgery as "Uninjured" data.
▲, additional MRI was performed before surgery as "Uninjured" data.

**Table S2. NT3-chitosan monkeys' detailed information (bedsore rate: 10.53%).**

| Monkey | Type | Bed-sore | Dead time post-surgery | Cause of death | Electro-physiology | MRI | Behavioral analysis | Histology | Regenerated (Histology/MRI/ Behavior) |
|---|---|---|---|---|---|---|---|---|---|
| #13▲ | NT3-chitosan | No | 2 years | Perfusion | No | Yes | No | Yes | Yes |
| #14 | NT3-chitosan | No | 3 years and 6 months | Perfusion | No | No | Yes | Yes | Yes |
| #15 | NT3-chitosan | Yes | 2 years and 2 months | Perfusion | No | No | No | Yes | Yes |
| #16▲ | NT3-chitosan | No | 3 years | Perfusion | No | Yes | No | Yes | Yes |
| #17 | NT3-chitosan | No | 1 year and 10 months | Perfusion | No | Yes | No | Yes | Yes |
| #18 | NT3-chitosan | No | 2 years and 3 months | Perfusion | No | No | Yes | Yes | Yes |
| #19 | NT3-chitosan | N/A | Death during surgery | Respiratory depression | N/A | N/A | N/A | N/A | N/A |
| #20▲ | NT3-chitosan | Yes | 5 months | Unknown | No | Yes | No | No | Unknown |
| #21 | NT3-chitosan | No | 3 years | Perfusion | No | No | Yes | Yes | Yes |
| #22 | NT3-chitosan | No | 3 years and 6 months | Perfusion | No | Yes | Yes | Yes | Yes |
| #23● | NT3-chitosan | No | 2 years and 1 month | Perfusion | Yes | No | No | Yes | Yes |
| #24● | NT3-chitosan | No | 1 year and 5 months | Perfusion | Yes | No | No | Yes | Yes |
| #25● | NT3-chitosan | No | 1 year and 9 months | Perfusion | Yes | No | No | Yes | Yes |
| #26● | NT3-chitosan | No | 2 years and 3 months | Perfusion | Yes | No | No | Yes | Yes |
| #27● | NT3-chitosan | No | 1 year and 3 months | Perfusion | Yes | No | No | Yes | Yes |
| #28 | NT3-chitosan | No | 1 year and 1 month | Perfusion | Yes | No | No | Yes | Yes |
| #35 | NT3-chitosan | No | 11 months | Perfusion | No | No | No | Yes | Yes |
| #36 | NT3-chitosan | No | 1 year and 3 months | Perfusion | No | No | No | Yes | Yes |
| #37 | NT3-chitosan | No | 2 years | Perfusion | No | No | No | Yes | Yes |
| #38 | NT3-chitosan | No | 1 years | Perfusion | No | No | No | Yes | Yes |

▲, additional MRI was performed before surgery as "Uninjured" data.

●, electrophysiological re-section experiments were performed for Figs. 3 and 4.

**Table S3. Uninjured monkeys' detailed information (used for Electrophysiology).**

| Monkey | Type | Bed-sore | Dead time post-surgery | Cause of death | Electro-Physiology | MRI | Behavioral analysis | Histology | Regenerated (Histology/MRI/ Behavior) |
|---|---|---|---|---|---|---|---|---|---|
| #29 | Uninjured | No | N/A | Perfusion | Yes | No | No | Yes | N/A |
| #30 | Uninjured | No | N/A | Perfusion | Yes | No | No | Yes | N/A |
| #31 | Uninjured | No | N/A | N/A | Yes | No | No | No | N/A |
| #32 | Uninjured | No | N/A | N/A | Yes | No | No | No | N/A |
| #33 | Uninjured | No | N/A | N/A | Yes | No | No | No | N/A |
| #34 | Uninjured | No | N/A | N/A | Yes | No | No | No | N/A |

**Table S4. Detailed information of the regenerated neural "bridge/funnel-like" tissues with diameters at the two "funnel" ends as well as at the center of the structure measured. In addition, "density indexes" of neurofilament staining within regenerated neural tissues from four representative NT3-chitosan animals were presented.**

| Monkey | Type | "Bridge" tissue diameters (mm) | | |
|---|---|---|---|---|
| | | Rostral | Middle | Caudal |
| #13 | NT3-chitosan | 2.00 | 1.00 | 1.90 |
| #14 | NT3-chitosan | 1.80 | 1.00 | 1.80 |
| #15 | NT3-chitosan | 2.10 | 1.00 | 1.80 |
| #17 | NT3-chitosan | 2.20 | 1.20 | 2.00 |
| #24 | NT3-chitosan | 1.90 | 1.00 | 2.10 |
| #27 | NT3-chitosan | 1.80 | 1.40 | 2.00 |
| #28 | NT3-chitosan | 2.10 | 1.20 | 2.00 |
| #35 | NT3-chitosan | 1.90 | 1.30 | 2.10 |
| #36 | NT3-chitosan | 2.30 | 1.30 | 2.10 |
| | | Density index (mean ± SEM) | | |
| #27 | NT3-chitosan | 0.3864 ± 0.0084 | | |
| #35 | NT3-chitosan | 0.3672 ± 0.0093 | | |
| #36 | NT3-chitosan | 0.4038 ± 0.0086 | | |
| #37 | NT3-chitosan | 0.4219 ± 0.0101 | | |

**Note:** lesion control group did not have bridge formation or neurofilament staining within lesion area.

**Table S5. Detailed information of analyzed kinematical parameters. The performance of bilateral hindlimbs in each gait cycle was recorded and calculated to obtain 127 gait parameters.**

| Parameters | Num | Detailes |
|---|---|---|
| Gait timing | | |
| | 1 | Left Cycle duration |
| | 2 | Right Cycle duration |
| | 3 | Left Stance duration |
| | 4 | Right Stance duration |
| | 5 | Left Swing duration |
| | 6 | Right Swing duration |
| | 7 | Left Working coefficient |
| | 8 | Right Working coefficient Right |
| | 9 | Right Dragging duration Right |
| | 10 | Right Relative dragging duration (percent of cycle duration) |
| Endpoint trajectory | | |
| | 11 | Left Stride length |
| | 12 | Right Stride length |
| | 13 | Left Step height |
| | 14 | Right Step height |
| | 15 | Left Limb endpoint trajectory length |
| | 16 | Right Limb endpoint trajectory length |
| | 17 | Left Max backward limb endpoint position |
| | 18 | Right Max backward limb endpoint position |
| | 19 | Left Max forward limb endpoint position |
| | 20 | Right Max forward limb endpoint position |
| | 21 | Left Max limb endpoint velocity |
| | 22 | Right Max limb endpoint velocity |
| | 23 | Left Limb endpoint velocity at beginning forward |
| | 24 | Right Limb endpoint velocity at beginning forward |
| | 25 | Left Limb endpoint velocity vector orientation at beginning forward |
| | 26 | Right Limb endpoint velocity vector orientation at beginning forward |
| | 27 | Left Limb endpoint acceleration at beginning forward |
| | 28 | Right Limb endpoint acceleration at beginning forward |
| Joint angles | | |
| | 29 | Left Knee joint extension |
| | 30 | Left Knee joint flexion |
| | 31 | Left Knee joint amplitude |
| | 32 | Right Knee joint extension |
| | 33 | Right Knee joint flexion |
| | 34 | Right Knee joint amplitude |
| | 35 | Left Ankle joint extension |
| | 36 | Left Ankle joint flexion |
| | 37 | Left Ankle joint amplitude |
| | 38 | Right Ankle joint extension |
| | 39 | Right Ankle joint flexion |
| | 40 | Right Ankle joint amplitude |
| Joint angular velocity | | |
| | 41 | Left Max Knee extension joint angular velocity |
| | 42 | Left Min Knee extension joint angular velocity |
| | 43 | Left Knee extension joint angular velocity amplitude |
| | 44 | Left Max Knee flexion joint angular velocity |
| | 45 | Left Min Knee flexion joint angular velocity |

| | | |
|---|---|---|
| | 46 | Left Knee flexion joint angular velocity amplitude |
| | 47 | Right Max Knee extension joint angular velocity |
| | 48 | Right Min Knee extension joint angular velocity |
| | 49 | Right Knee extension joint angular velocity amplitude |
| | 50 | Right Max Knee flexion joint angular velocity |
| | 51 | Right Min Knee flexion joint angular velocity |
| | 52 | Right Knee flexion joint angular velocity amplitude |
| | 53 | Left Max Ankle extension joint angular velocity |
| | 54 | Left Min Ankle extension joint angular velocity |
| | 55 | Left Ankle extension joint angular velocity amplitude |
| | 56 | Left Max Ankle flexion joint angular velocity |
| | 57 | Left Min Ankle flexion joint angular velocity |
| | 58 | Left Ankle flexion joint angular velocity amplitude |
| | 59 | Right Max Ankle extension joint angular velocity |
| | 60 | Right Min Ankle extension joint angular velocity |
| | 61 | Right Ankle extension joint angular velocity amplitude |
| | 62 | Right Max Ankle flexion joint angular velocity |
| | 63 | Right Min Ankle flexion joint angular velocity |
| | 64 | Right Ankle flexion joint angular velocity amplitude |
| Hindlimb oscillations | | |
| | 65 | Left Limb axis amplitude |
| | 66 | Right Limb axis amplitude |
| | 67 | Left Mean limb axis velocity |
| | 68 | Right Mean limb axis velocity |
| Intra-hindlimb coordinations | | |
| | 69 | Left Correlation between knee and ankle joint |
| | 70 | Right Correlation between knee and ankle joint |
| | 71 | Left Correlation between hip and knee heights |
| | 72 | Right Correlation between hip and knee heights |
| | 73 | Left Correlation between hip and ankle heights |
| | 74 | Right Correlation between hip and ankle heights |
| | 75 | Left Correlation between hip and toe heights |
| | 76 | Right Correlation between hip and toe heights |
| | 77 | Left Correlation between knee and ankle heights |
| | 78 | Right Correlation between knee and ankle heights |
| | 79 | Left Correlation between knee and toe heights |
| | 80 | Right Correlation between knee and toe heights |
| | 81 | Left Correlation between ankle and toe heights |
| | 82 | Right Correlation between ankle and toe heights |
| | 83 | Left Max altitude difference between hip and knee |
| | 84 | Left Min altitude difference between hip and knee |
| | 85 | Left Amplitude of altitude difference between hip and knee |
| | 86 | Right Max altitude difference between hip and knee |
| | 87 | Right Min altitude difference between hip and knee |
| | 88 | Right Amplitude of altitude difference between hip and knee |
| | 89 | Left Max altitude difference between hip and ankle |
| | 90 | Left Min altitude difference between hip and ankle |
| | 91 | Left Amplitude of altitude difference between hip and ankle |
| | 92 | Right Max altitude difference between hip and ankle |
| | 93 | Right Min altitude difference between hip and ankle |
| | 94 | Right Amplitude of altitude difference between hip and ankle |
| | 95 | Left Max altitude difference between hip and toe |
| | 96 | Left Min altitude difference between hip and toe |
| | 97 | Left Amplitude of altitude difference between hip and toe |
| | 98 | Right Max altitude difference between hip and toe |

| | | |
|---|---|---|
| | 99 | Right Min altitude difference between hip and toe |
| | 100 | Right Amplitude of altitude difference between hip and toe |
| | 101 | Left Max altitude difference between knee and ankle |
| | 102 | Left Min altitude difference between knee and ankle |
| | 103 | Left Amplitude of altitude difference between knee and ankle |
| | 104 | Right Max altitude difference between knee and ankle |
| | 105 | Right Min altitude difference between knee and ankle |
| | 106 | Right Amplitude of altitude difference between knee and ankle |
| | 107 | Left Max altitude difference between knee and toe |
| | 108 | Left Min altitude difference between knee and toe |
| | 109 | Left Amplitude of altitude difference between knee and toe |
| | 110 | Right Max altitude difference between knee and toe |
| | 111 | Right Min altitude difference between knee and toe |
| | 112 | Right Amplitude of altitude difference between knee and toe |
| | 113 | Left Max altitude difference between ankle and toe |
| | 114 | Left Min altitude difference between ankle and toe |
| | 115 | Left Amplitude of altitude difference between ankle and toe |
| | 116 | Right Max altitude difference between ankle and toe |
| | 117 | Right Min altitude difference between ankle and toe |
| | 118 | Right Amplitude of altitude difference between ankle and toe |
| Inter-hindlimb coordinations | | |
| | 119 | Left-Right Swing phase correlation value |
| | 120 | Right Working coefficient / Left Working coefficient |
| Stability | | |
| | 121 | Left-Right Average stand width |
| | 122 | Left Pelvis oscillations in the left-right axis |
| | 123 | Left Pelvis oscillations in the anterior-posterior axis |
| | 124 | Left Pelvis oscillations in the superior-inferior axis |
| | 125 | Right Pelvis oscillations in the left-right axis |
| | 126 | Right Pelvis oscillations in the anterior-posterior axis |
| | 127 | Right Pelvis oscillations in the superior-inferior axis |

**Table S6. Datasets of the gait parameters and the lesion size.**

| Group | No. | LS-1 | LS-2 | LS-3 | LS-4 | GP-1 | GP-2 | GP-3 | GP-4 | GP-5 | GP-6 | GP-7 | GP-8 | GP-9 | GP-10 | GP-11 | GP-12 |
|---|---|---|---|---|---|---|---|---|---|---|---|---|---|---|---|---|---|
| LC | #1 | 24.300 | 20.335 | 58.919 | 0.345 | 0.840 | 0.250 | 126.730 | 0.000 | 0.000 | 403.121 | 0.000 | 0.000 | 10.765 | 3.175 | 501.203 | 0.111 |
| | #5 | 24.600 | 21.695 | 52.219 | 0.415 | 0.336 | 0.233 | 155.651 | 0.424 | 0.160 | 265.413 | 0.236 | 0.459 | 19.367 | 20.413 | 319.118 | 0.056 |
| | #6 | 26.600 | 21.823 | 65.411 | 0.334 | 0.450 | 0.274 | 184.956 | 0.411 | 0.140 | 333.833 | 0.231 | 0.374 | 21.002 | 29.306 | 339.745 | 0.058 |
| NT3 | #14 | 27.000 | 23.642 | 36.868 | 0.641 | 0.096 | 0.068 | 58.458 | 0.953 | 0.329 | 414.298 | 0.666 | 1.023 | 44.863 | 61.528 | 628.758 | 0.228 |
| | #18 | 23.800 | 21.521 | 39.182 | 0.549 | 0.048 | 0.021 | 99.941 | 0.927 | 0.331 | 427.817 | 0.524 | 1.404 | 50.825 | 77.842 | 586.237 | 0.096 |
| | #21 | 23.400 | 23.741 | 42.709 | 0.556 | 0.075 | 0.062 | 80.398 | 0.762 | 0.482 | 433.464 | 0.907 | 1.802 | 22.393 | 67.619 | 497.069 | 0.130 |
| | #22 | 24.500 | 23.610 | 47.836 | 0.494 | 0.000 | 0.000 | 42.477 | 1.779 | 0.270 | 523.346 | 0.593 | 1.082 | 54.498 | 122.158 | 891.310 | 0.143 |

**Note:** LC, lesion control; NT3, NT3-chitosan group;
LS-1, Original lesion size ($mm^2$);
LS-2, Final lesion size (framed by white line) ($mm^2$);
LS-3, Area of ROI (framed by red line) ($mm^2$);
LS-4, Relative of final lesion size (a.u.);
GP-1, Right dragging duration (s);
GP-2, Right relative dragging duration (% of cycle duration) (a.u.);
GP-3, Left-right average stand width (mm);
GP-4, Right stance phase duration (s);
GP-5, Right working coefficient (a.u.);
GP-6, Right stride length (mm);
GP-7, Right swing phase duration (s);
GP-8, Right working coefficient/Left working coefficient (a.u.);
GP-9, Right ankle joint amplitude (deg);
GP-10, Right step height (mm);
GP-11, Right limb endpoint trajectory length (mm);
GP-12, Right limb endpoint velocity at beginning forward (m/s).

**Table S7. Statistical results of the correlations between the gait parameters and the lesion size.**

*Hypothesis: Within our SCI model, the bigger the lesion area, the worse the functional outcomes.*

| Gait parameters | Original lesion size | | | Final lesion size | | | Relative of final lesion size | | |
|---|---|---|---|---|---|---|---|---|---|
| | ***P* value** | ***r*** | ***Correlation to hypothesis*** | ***P* value** | ***r*** | ***Correlation to hypothesis*** | ***P* value** | ***r*** | ***Correlation to hypothesis*** |
| Right dragging duration (s) | 0.8508 | 0.0883 | Not correlated | **0.0307*** | **-0.8000** | "-" | **0.0292*** | **-0.8043** | "-" |
| Right relative dragging duration (% of cycle duration) (a.u.) | 0.5238 | 0.2929 | Not correlated | **0.0959** | **-0.6754** | "-" | **0.0185*** | **-0.8381** | "-" |
| Left-right average stand width (mm) | 0.6971 | 0.1814 | Not correlated | **0.0829** | **-0.6953** | "-" | **0.0347*** | **-0.7896** | "-" |
| Right stance phase duration (s) | 0.9176 | -0.0486 | Not correlated | **0.0583** | **0.7379** | "-" | 0.1629 | 0.5903 | Not correlated |
| Right working coefficient (a.u.) | 0.6329 | -0.2216 | Not correlated | **0.0324*** | **0.7955** | "-" | **0.0190*** | **0.8364** | "-" |
| Right stride length (mm) | 0.5753 | -0.2587 | Not correlated | 0.2727 | 0.4826 | Not correlated | 0.2913 | 0.4665 | Not correlated |
| Right swing phase duration (s) | 0.7325 | -0.1596 | Not correlated | **0.0080**** | **0.8855** | "-" | **0.0155*** | **0.8497** | "-" |
| Right working coefficient /Left working coefficient (a.u.) | 0.4100 | -0.3729 | Not correlated | **0.0716** | **0.7139** | "-" | **0.0300*** | **0.8020** | "-" |
| Right ankle joint amplitude (deg) | 0.8885 | 0.0658 | Not correlated | 0.2324 | 0.5192 | Not correlated | **0.0957** | **0.6757** | "-" |
| Right step height (mm) | 0.7020 | -0.1784 | Not correlated | **0.0681** | **0.7200** | "-" | 0.1349 | 0.6232 | Not correlated |
| Right limb endpoint trajectory length (mm) | 0.7982 | -0.1197 | Not correlated | 0.2442 | 0.5082 | Not correlated | 0.2499 | 0.5030 | Not correlated |
| Right limb endpoint velocity at beginning forward (m/s) | 0.5035 | 0.3067 | Not correlated | 0.1331 | 0.6254 | Not correlated | **0.0464*** | **0.7621** | "-" |

+: positively correlated with the hypothesis (agree with the hypothesis); -: negatively correlated with the hypothesis (disagree with the hypothesis).

**Table S8. Statistical results of the correlations between the gait parameters and the lesion size in LC group.**

*Hypothesis: Within our SCI model, the bigger the lesion area, the worse the functional outcomes.*

| Gait parameters | Original lesion size | | | Final lesion size | | | Relative of final lesion size | | |
|---|---|---|---|---|---|---|---|---|---|
| | ***P* value** | ***r*** | ***Correlation to hypothesis*** | ***P* value** | ***r*** | ***Correlation to hypothesis*** | ***P* value** | ***r*** | ***Correlation to hypothesis*** |
| Right dragging duration (s) | 0.7278 | -0.4147 | Not correlated | 0.1871 | -0.9571 | Not correlated | 0.6120 | -0.5725 | Not correlated |
| Right relative dragging duration (% of cycle duration) (a.u.) | 0.3525 | 0.8506 | Not correlated | 0.8932 | 0.1670 | Not correlated | 0.3078 | -0.8854 | Not correlated |
| Left-right average stand width (mm) | 0.2544 | 0.9212 | Not correlated | 0.2863 | 0.9006 | Not correlated | 0.9146 | -0.1337 | Not correlated |
| Right stance phase duration (s) | 0.6080 | 0.5776 | Not correlated | **0.0673** | **0.9944** | "-" | 0.7318 | 0.4090 | Not correlated |
| Right working coefficient (a.u.) | 0.6621 | 0.5062 | Not correlated | 0.1215 | 0.9819 | Not correlated | 0.6776 | 0.4851 | Not correlated |
| Right stride length (mm) | 0.9211 | -0.1236 | Not correlated | 0.3804 | -0.8267 | Not correlated | 0.4186 | -0.7915 | Not correlated |
| Right swing phase duration (s) | 0.6018 | 0.5855 | Not correlated | **0.0611** | **0.9954** | "-" | 0.7379 | 0.4001 | Not correlated |
| Right working coefficient /Left working coefficient (a.u.) | 0.7007 | 0.4530 | Not correlated | 0.1600 | 0.9686 | Not correlated | 0.6390 | 0.5371 | Not correlated |
| Right ankle joint amplitude (deg) | 0.4951 | 0.7125 | Not correlated | **0.0455*** | **0.9974** | "-" | 0.8446 | 0.2417 | Not correlated |
| Right step height (mm) | 0.3728 | 0.8334 | Not correlated | 0.1678 | 0.9654 | Not correlated | 0.9669 | 0.0520 | Not correlated |
| Right limb endpoint trajectory length (mm) | 0.6561 | -0.5143 | Not correlated | 0.1154 | 0.9836 | Not correlated | 0.6836 | -0.4767 | Not correlated |
| Right limb endpoint velocity at beginning forward (m/s) | 0.6046 | -0.5820 | Not correlated | **0.0639** | **-0.9950** | "+" | 0.7352 | -0.4041 | Not correlated |

+: agree with the hypothesis; -: disagree with the hypothesis.

**Table S9. Statistical results of the correlations between the gait parameters and the lesion size in NT3 group.**

*Hypothesis: Within our SCI model, the bigger the lesion area, the worse the functional outcomes.*

| Gait parameters | Original lesion size | | | Final lesion size | | | Relative of final lesion size | | |
|---|---|---|---|---|---|---|---|---|---|
| | ***P* value** | ***r*** | ***Correlation to hypothesis*** | ***P* value** | ***r*** | ***Correlation to hypothesis*** | ***P* value** | ***r*** | ***Correlation to hypothesis*** |
| Right dragging duration (s) | 0.5776 | 0.4224 | Not correlated | 0.8626 | 0.1374 | Not correlated | **0.0814** | **0.9186** | "+" |
| Right relative dragging duration (% of cycle duration) (a.u.) | 0.6224 | 0.3776 | Not correlated | 0.6350 | 0.3650 | Not correlated | 0.1569 | 0.8431 | Not correlated |
| Left-right average stand width (mm) | 0.4952 | -0.5048 | Not correlated | 0.2469 | -0.7531 | Not correlated | 0.8855 | 0.1145 | Not correlated |
| Right stance phase duration (s) | 0.9449 | 0.0551 | Not correlated | 0.7811 | 0.2189 | Not correlated | 0.3564 | -0.6436 | Not correlated |
| Right working coefficient (a.u.) | 0.5753 | -0.4247 | Not correlated | 0.7858 | 0.2142 | Not correlated | 0.8026 | 0.1974 | Not correlated |
| Right stride length (mm) | 0.7703 | -0.2297 | Not correlated | 0.7346 | 0.2654 | Not correlated | 0.1790 | -0.8210 | Not correlated |
| Right swing phase duration (s) | 0.7890 | -0.2110 | Not correlated | 0.3653 | 0.6347 | Not correlated | 0.8237 | 0.1763 | Not correlated |
| Right working coefficient /Left working coefficient (a.u.) | 0.2287 | -0.7713 | Not correlated | 0.9074 | -0.0926 | Not correlated | 0.8283 | -0.1717 | Not correlated |
| Right ankle joint amplitude (deg) | 0.6882 | 0.3118 | Not correlated | 0.5961 | -0.4039 | Not correlated | 0.7676 | -0.2324 | Not correlated |
| Right step height (mm) | 0.7543 | -0.2457 | Not correlated | 0.9243 | 0.0757 | Not correlated | 0.1570 | -0.8430 | Not correlated |
| Right limb endpoint trajectory length (mm) | 0.8062 | 0.1938 | Not correlated | 0.7910 | 0.2090 | Not correlated | 0.4694 | -0.5306 | Not correlated |
| Right limb endpoint velocity at beginning forward (m/s) | **0.0597** | **0.9403** | "-" | 0.3877 | 0.6123 | Not correlated | 0.2707 | 0.7293 | Not correlated |

+: agree with the hypothesis; -: disagree with the hypothesis.

**Table S10. Exacted numbers of animals and statistical comparison results of lesion extent between the lesion control group and the NT3-chitosan group in each experiment.**

| **Figures** | ***n* per group （condition）** | | |
|---|---|---|---|
| Fig. 3 | 6 (uninjured) | 6 (lesion control, LC) | 6 (NT3-chitosan, NT3)<br>(after examination, 2 recut intact and 3 recut renew tissues)<br>(lesion area comparsion: *P*=0.3947; LC vs NT3, two-tailed independent sample t-test, variance homogeneous) |
| Fig. 4 | 6 (uninjured) | 6 (lesion control, LC) | 6 (NT3-chitosan, NT3)<br>(after examination, 2 recut intact and 3 recut renew tissues)<br>(lesion area comparsion: *P*=0.3947; LC vs NT3, two-tailed independent sample t-test, variance homogeneous) |
| Fig. 5 | 5 (uninjured) | 3 (lesion control, LC) | 4 (NT3-chitosan, NT3)<br>(lesion area comparsion: *P*=0.8580; LC vs NT3, two-tailed independent sample t-test, variance homogeneous) |
| Fig. 6*E* | 5 (uninjured) | 3 (lesion control, LC) | 4 (NT3-chitosan, NT3)<br>(lesion area comparsion: *P*=0.6818; LC vs NT3, two-tailed independent sample t-test, variance homogeneous) |
| Fig. 7*E* | 5 (uninjured) | 3 (lesion control, LC) | 4 (NT3-chitosan, NT3) |
| Fig. 7*G* | / | 3 (lesion control,LC, 4 timepoints) | 4 (NT3-chitosan, NT3, 4 timepoints)<br>(lesion area comparsion: *P*=0.8580; LC vs NT3, two-tailed independent sample t-test, variance homogeneous) |

**Table S11. Exacted *P* values and statistical tests for each significant difference.**

| Figures | *P* value (comparison, test, estimate of variation) |
|---|---|
| Fig. 3 | 0.0097 (Amplititude, Right cortex: Uninjured vs NT3-chitosan, ANOVA with Bonferroni, variance homogeneous) |
| | <0.0001 (Amplititude, Right cortex: Uninjured vs Lesion control, ANOVA with Bonferroni, variance homogeneous) |
| | 0.0419 (Amplititude, Right cortex: NT3-chitosan vs Lesion control, ANOVA with with Bonferroni, variance homogeneous) |
| | 0.0004 (Amplititude, Left cortex: Uninjured vs NT3-chitosan, two-tailed Independent Sample T-Test, variance homogeneous) |
| Fig. 4 | 0.0052(contralateral: Amplititude, Left hindlimb: Uninjured vs NT3-chitosan, ANOVA with Bonferroni, variance homogeneous) |
| | <0.0001 (contralateral: Amplititude, Left hindlimb: Uninjured vs Lesion control, ANOVA with Bonferroni, variance homogeneous) |
| | 0.0004 (contralateral: Amplititude, Left hindlimb: NT3-chitosan vs Lesion control, ANOVA with Bonferroni, variance homogeneous) |
| | <0.0001 (contralateral: Amplititude, Right hindlimb: Uninjured vs NT3-chitosan, two-tailed Independent Sample T-Test, variance homogeneous) |
| | 0.0341 (contralateral: Latency, Right hindlimb: Uninjured vs NT3-chitosan, two-tailed Independent Sample T-Test, variance inhomogeneous) |
| | 0.0091 (ipsilateral: Amplititude, Left hindlimb: Uninjured vs Lesion control, ANOVA with Bonferroni, variance homogeneous) |
| | 0.0252 (ipsilateral: Amplititude, Left hindlimb: NT3-chitosan vs Lesion control, ANOVA with Bonferroni, variance homogeneous) |
| | 0.0006 (ipsilateral: Amplititude, Right hindlimb: Uninjured vs NT3-chitosan, two-tailed Independent Sample T-Test, variance inhomogeneous) |
| | 0.0461 (ipsilateral: Latency, Right hindlimb: Uninjured vs NT3-chitosan, two-tailed Independent Sample T-Test, variance homogeneous) |
| Fig. 5 | 0.0031 (Uninjured① vs Lesion control②, ANOVA with Bonferroni, variance homogeneous) |
| | 0.0086 (Lesion control② vs NT3-chitosan③, ANOVA with Bonferroni, variance homogeneous) |
| Fig. 6*E* | <0.0001 (Right dragging duration: Lesion control vs NT3-chitosan, two-tailed Mann-Whitney U-test, N/A) |
| | <0.0001 (Right relative dragging duration: Lesion control vs NT3-chitosan, two-tailed Mann-Whitney U-test, N/A) |
| | <0.0001 (Left-right average stand width: Uninjured vs Lesion control, Kruskal-Wallis, N/A) |
| | <0.0001 (Left-right average stand width: Lesion control vs NT3-chitosan, Kruskal-Wallis, N/A) |
| | <0.0001 (Right stance phase duration: Uninjured vs Lesion control, Kruskal-Wallis, N/A) |
| | <0.0001 (Right stance phase duration: Lesion control vs NT3-chitosan, Kruskal-Wallis, N/A) |
| | <0.0001 (Right working coefficient: Uninjured vs Lesion control, Kruskal-Wallis, N/A) |
| | <0.0001 (Right working coefficient: Lesion control vs NT3-chitosan, Kruskal-Wallis, N/A) |
| | 0.0001 (Right stride length: Uninjured vs Lesion control, ANOVA with Dunnetts' T3, variance inhomogeneous) |
| | <0.0001 (Right stride length: Lesion control vs NT3-chitosan, ANOVA with Dunnetts' T3, variance inhomogeneous) |
| | <0.0001 (Right swing phase duration: Uninjured vs Lesion control, Kruskal-Wallis, N/A) |
| | <0.0001 (Right swing phase duration: Lesion control vs NT3-chitosan, Kruskal-Wallis, N/A) |
| | <0.0001 (Right working coefficient/Left working coefficient: Uninjured vs Lesion control, Kruskal-Wallis, N/A) |
| | <0.0001 (Right working coefficient/Left working coefficient: Lesion control vs NT3-chitosan, Kruskal-Wallis, N/A) |
| | <0.0001 (Right ankle joint amplitude: Uninjured vs Lesion control, ANOVA with Dunnetts' T3, variance inhomogeneous) |
| | <0.0001 (Right ankle joint amplitude: Lesion control vs NT3-chitosan, ANOVA with Dunnetts' T3, variance inhomogeneous) |
| | 0.001 (Right step height: Uninjured vs Lesion control, Kruskal-Wallis, N/A) |
| | <0.0001 (Right step height: Lesion control vs NT3-chitosan, Kruskal-Wallis, N/A) |
| | <0.0001 (Right step height: Uninjured vs NT3-chitosan, Kruskal-Wallis, N/A) |
| | <0.0001 (Right limb endpoint trajectory length: Uninjured vs Lesion control, Kruskal-Wallis, N/A) |
| | <0.0001 (Right limb endpoint trajectory length: Lesion control vs NT3-chitosan, Kruskal-Wallis, N/A) |
| | <0.0001 (Right limb endpoint velocity at beginning forward: Uninjured vs Lesion control, Kruskal-Wallis, N/A) |
| | 0.0006 (Right limb endpoint velocity at beginning forward: Lesion control vs NT3-chitosan, Kruskal-Wallis, N/A) |

| | |
|---|---|
| Fig. 7*E* | <0.0001 (FA values in Rostral-Caudal direction: Uninjured vs Lesion control, ANOVA with Dunnetts' T3, variance inhomogeneous) |
| | 0.0029 (FA values in Rostral-Caudal direction: Lesion control vs NT3-chitosan, ANOVA with Dunnetts' T3, variance inhomogeneous) |
| | <0.0001 (FA values in Rostral-Caudal direction: Uninjured vs NT3-chitosan, ANOVA with Dunnetts' T3, variance inhomogeneous) |
| | <0.0001 (% of Rostral-Caudal voxels: Uninjured vs Lesion control, ANOVA with Bonferroni, variance homogeneous) |
| | 0.0292 (% of Rostral-Caudal voxels: Lesion control vs NT3-chitosan, ANOVA with Bonferroni, variance homogeneous) |
| | 0.0002 (% of Rostral-Caudal voxels: Uninjured vs NT3-chitosan, ANOVA with Bonferroni, variance homogeneous) |
| Fig. 7*G* | 0.0418 (FA values in surgical site: Lesion control vs NT3-chitosan, two-tailed Independent Sample T-Test, variance homogeneous) |
| | 0.0451 (FA values in surgical site: Lesion control vs NT3-chitosan, two-way ANOVA with Bonferroni, variance homogeneous) |
| | 0.0012 (% of Rostral-Caudal voxels in surgical site: Lesion control vs NT3-chitosan, two-tailed Independent Sample T-Test, variance homogeneous) |
| | 0.0153 (% of Rostral-Caudal voxels in surgical site: Lesion control vs NT3-chitosan, two-way ANOVA with Bonferroni, variance homogeneous) |

**Movie S1. Gait performance in three animals (Uninjured, Lesion control, and NT3-chitosan). This video displays continuous stepping of an uninjured monkey, a lesion control monkey (6 months after SCI), and a NT3-chitosan implanted monkey (6 months after SCI).**

**References**


1. Yang ZY, Zhang AF, Duan HM, Zhang S, Hao P, Ye KQ, Sun YE, Li XG. (2015) NT3-choitsan elicits robust endogenous neurogenesis to enable functional recovery after spinal cord injury. *Proc Natl Acad Sci USA* 112:13354-13359.
2. Li XG, Yang ZY, Zhang AF, Wang TL, Chen WC (2009b) Repair of thoracic spinal cord injury by chitosan tube implantation in adult rats. *Biomaterials* 30:1121-1132.
3. Rosenzweig ES, Brock JH, Culbertson MD; Lu P, Moseanko R, Edgerton VR , Havton LA, Tuszynski MH (2009) Extensive spinal decussation and bilateral termination of cervical corticospinal projections in rhesus monkeys. *J Comp Neurol* 513:151-163.
4. Petersen JA, Wilm BJ, Von Meyenburg J, Schubert M, Seifert B, Najafi Y, Dietz V, Kollias S (2012) Chronic cervical spinal cord injury: DTI correlates with clinical and electrophysiological measures. *J Neurotrauma* 29:1556-1566.
5. Yang ZY, Mo LH, Duan HM, Li XG (2010) Effects of chitosan/collagen substrates on the behavior of rat neural stem cells. *Sci China-Life Sci* 53:215-222.
6. Luft AR, Kaelin-Lang A, Hauser TK, Cohen LG, Thakor NV, Hanley DF (2001) Transcranial magnetic stimulation in the rat. *Exp Brain Res* 140:112-121.
7. Vincent JL, Patel GH, Fox MD, Snyder AZ, Baker JT, Van Essen DC, Zempel JM, Snyder LH, Corbetta M, Raichle ME (2007) Intrinsic functional architecture in the anaesthetized monkey brain. *Nature* 447:83-86.
8. Rao JS, Liu ZX, Zhao C, Wei RH, Zhao W, Tian PY, Zhou X, Yang ZY, Li XG (2017) Ketamine changes the local resting-state functional properties of anesthetized-monkey brain. *Magn Reson Imaging* 43: 144-150.
9. Rao JS, Ma MX, Zhao C, Xi Y, Yang ZY, Liu ZX, Li XG (2013) Atrophy and primary somatosensory cortical reorganization after unilateral thoracic spinal cord injury: A longitudinal functional magnetic resonance imaging study. *BioMed Res Int* 1, Article ID 753061.
10. Reese TG, Heid O, Weisskoff RM, Wedeen VJ (2003) Reduction of eddy-current-induced distortion in diffusion MRI using a twice-refocused spin echo. *Magn Reson Med* 49:177-182.
11. Rao JS, Zhao C, Yang ZY, Li SY, Jiang T, Fan YB, Li XG (2013) Diffusion tensor tractography of residual fibers in traumatic spinal cord injury: A pilot study. *J Neuroradiol* 40:181-186.
12. Basser PJ, Mattiello J, LeBihan D (1994) MR diffusion tensor spectroscopy and imaging. *Biophys J* 66:259-267.
13. Friston KJ, Ashburner J, Frith CD, Poline J-B, Heather JD, Frackowiak RSJ (1995) Spatial registration and normalization of images. *Hum Brain Mapp* 2:165-189.
14. McLaren DG, Kosmatka KJ, Oakes TR, Kroenke CD, Kohama SG, Matochik JA, Ingram DK, Johnso SC (2009) A population-average MRI-based atlas collection of the rhesus macaque. *NeuroImage* 45:52-59.
15. Rohlfing T, Kroenke CD, Sullivan EV, Dubach MF, Bowden DM, Grant KA, Pfefferbaum1 A (2012) The INIA19 template and neuromaps atlas for primate brain image parcellation and spatial normalization. *Front Neuroinform* 6:1-15.
16. Wey HY, Li J, Szabó CA, Fox PT, Leland MM, Jones L, Duong TQ (2010) BOLD fMRI of visual and somatosensory-motor stimulations in baboons. *NeuroImage* 52:1420-1427.

17. Saleem KS, Logothetis NK (2007) A combined MRI and histology atlas of the rhesus monkey brain in stereotaxic coordinates (New York: Academic Press, NY).
18. Zhao C, Rao JS, Pei XJ, Lei JF, Wang ZJ, Zhao W, Wei RH, Yang ZY, Li XG (2018) Diffusion tensor imaging of spinal cord parenchyma lesion in rat with chronic spinal cord injury. *Magn Reson Imaging* 47:25-32.
19. Zhao C, Rao JS, Pei XJ, Lei JF, Wang ZJ, Yang ZY, Li XG (2016) Longitudinal study on diffusion tensor imaging and diffusion tensor tractography following spinal cord contusion injury in rats. *Neuroradiology* 58:607-614.
20. Wei RH, Song W, Zhao C, Zhao W, Li LF, Ji R, Rao JS, Yang ZY, Li XG (2016) Influence of walking speed on gait parameters of bipedal locomotion in rhesus monkeys. *J Med Primatol* 45:304-311.
21. Zhao C, Song W, Rao JS, Zhao W, Wei RH, Zhou X, Tian PY, Yang ZY, Li XG (2017) Combination of kinematic analyses and diffusion tensor tractrography to evaluate the residual motor functions in spinal cord-hemisected monkeys. *J Med Primatol* 46:239-247.
22. Zhao W, Song W, Rao JS, Wei RH, Li LF, Ji R, Zhao C, Yang ZY, Li XG (2018) Gait division of healthy and spinal cord-injured Rhesus monkeys by one-dimensional toe signals. *J Mech Med Biol* 18: 1850017.
23. Langfelder P, Horvath S (2008) WGCNA: an R package for weighted correlation network analysis. *BMC Bioinformatics* 9, Article ID 559.
24. Shirasaki DI, Greiner ER, Al-Ramahi I, Gray M, Boontheung P, Geschwind DH, Botas J, Coppola G, Horvath S, Loo JA, Yang XW (2012) Network organization of the Huntingtin proteomic interactome in mammalian brain. *Neuron* 75:41-57.
25. Zhang B, Horvath S (2005) A general framework for weighted gene co-expression network analysis. *Appl Genet Mol Biol* 4:1-45.